nature communications

Article

https://doi.org/10.1038/s41467-025-58896-y

Innate network mechanisms of temporal pole for semantic cognition in neonatal and adult twin studies

Received: 2 August 2024

Accepted: 4 April 2025

Published online: 23 April 2025

Check for updates

Ziliang Zhu[1,9], Huichao Yang[2,9], Haojie Wen[3], Jinyi Hung[4], Yueqin Hu[5], Yanchao Bi[1,6,7,8] ✉ & Xi Yu[1] ✉

What are the innate neural mechanisms scaffolding the protracted development of sophisticated human cognition observable later in life? We investigate this question by focusing on the putative hub of the human semantic memory system—the temporal pole. Combining infant- and twin-based imaging analyses, we examine the ontogenetic mechanisms and network characteristics of the functional subdivisions within the temporal pole that are specialized for semantic processing of different types in adults. Our findings reveal topologically similar temporal pole parcellations in the adult and neonatal brains. Notably, the specific functional connectivity of the dorsal and ventrolateral subdivisions with semantic-related networks are evident in neonates, significantly heritable, and associated with semantic functions in adult twins. These results demonstrate the neonatal emergence of genetically programmed functional connectivity characteristics in the temporal pole parcellations that underlie its crucial role in semantic processing, highlighting the innate network mechanisms that support semantic cognition in humans.

Understanding the origins of higher-order human cognition has long been central to philosophical, biological, and psychological inquiries[1–3]. Leveraging natural variations in complex behaviors observable in developed populations, twin-based studies and recently available genome-wide association studies (GWAS) have identified heritable cognitive and neural mechanisms underlying sophisticated abilities, such as reasoning[4] and language[5–7]. These findings underscore the genetic contributions to higher-order cognitive abilities that develop over time and are influenced by environmental factors. To elucidate the innate brain foundations of human cognition that are present and functional in the first applicable scenario[3,8], direct examinations of ontogenetic mechanisms are crucial. Previous research on infant behavior has identified rudimentary cognitive capacities with signature limits that enable recognition and processing of the physical world shortly after birth (i.e., core knowledge systems[3]). Advances in infant imaging techniques now allow for the in vivo characterization of macrofunctional brain organization in newborns with minimal postnatal experience. This facilitates the identification of the early-emerging neural mechanisms underlying complex cognitive functions observable later in life. By applying a genetic-based approach, we can link heritable patterns in early neural characteristics to functional differences observed in adults. Together, these techniques have the potential to provide direct evidence for innate brain mechanisms that scaffold the postnatal development of complex abilities. Here, we employ this combinatory approach to investigate the innate functional structure

[1]State Key Laboratory of Cognitive Neuroscience and Learning, Beijing Normal University, Beijing, China. [2]College of Education, Hebei Normal University, Shijiazhuang, China. [3]School of Systems Science, Beijing Normal University, Beijing, China. [4]Department of Audiology and Speech-Language Pathology, Mackay Medical College, New Taipei City, Taiwan. [5]Faculty of Psychology, Beijing Normal University, Beijing, China. [6]School of Psychological and Cognitive Science and Key Laboratory of Machine Perception (Ministry of Education), Peking University, Beijing, China. [7]IDG/McGovern Institute for Brain Research, Peking University, Beijing, China. [8]Institute for Artificial Intelligence, Peking University, Beijing, China. [9]These authors contributed equally: Ziliang Zhu, Huichao Yang. ✉e-mail: ybi@pku.edu.cn; xi.yu@bnu.edu.cn

of the temporal pole (TP), a putative hub region in the semantic memory system.

The semantic memory system refers to the neurocognitive mechanisms underlying the representation of world knowledge in humans. It guides our interactions with others and the environment and, therefore, lies at the core of higher-order cognition. Semantic knowledge is built from information acquired through multiple modalities/situations, such as auditory, visual, language, and emotional experiences[9–12]. Extensive research involving adult participants has revealed that the semantic memory is encoded within a set of hierarchically organized and convergently connected cortical areas[9,12–14]. This neural architecture supports a wide range of semantic processes, ranging from modality-specific information representation grounded in widely distributed neural networks, to the integration of information and the formation of generalized concepts supported by the multimodal hub in the bilateral anterior temporal lobes (ATL, see ref. 12 for a review). The TP area, located at the rostral part of the ATL, plays a critical role in multimodal information integration, as evidenced by neuropsychological and transcranial magnetic stimulation studies[15–19]. Previous parcellation studies have identified connection-based functional subdivisions within the TP of the adult brain[20,21]. The dorsal TP primarily connects with the auditory cortices and perisylvian language areas, while the ventral TP is more closely associated with visual circuits[20–23]. An intermediate area, the (ventro)lateral TP, has also been delineated, showing predominant connectivity with the default and semantic networks[20,21,24,25]. The graded structure of the TP, along with the proposed distance-dependent connectivity patterns of its subdivisions[26], is theorized to support the integration of diverse information sources and the formation of generalized concepts[12,14,27].

Notably, all neurocognitive models of semantic representation emphasize the importance of postnatal experiences across various modalities and contents (e.g., speech and images) in the formation of semantic representation in the human brain. However, these models are mute regarding the neurodevelopmental origins that scaffold the accumulation of semantic knowledge. The neural mechanisms underlying semantic representation are shared across individuals with diverse cultural, linguistic, and sensory experiences[9,13,28,29], indicating a universal pattern. A few studies have begun to explore the potentially innate categorical organization within visual pathways. For instance, selective responses to faces and places have been observed in infants aged 2-10 months[30,31] and have shown significant genetic influences in adults[32]. Despite these findings, the developmental precursors of the putative hub role of the TP in the large-scale neural network of the semantic memory system are virtually unknown.

Leveraging open-source imaging datasets from the WU-Minn Human Connectome Project[33] (HCP) and the developing Human Connectome Project[34] (dHCP), the present study reveals the innate connectivity mechanisms underlying the role of the TP in semantic representation through the integration of infant imaging and twin-based approaches (see Table 1 for demographic and imaging data characteristics of all participant groups). In Study 1, we identified tripartite functional parcellations within the TP of the adult brain through data-driven parcellation analyses of resting-state functional connectivity (FC) patterns of unrelated HCP adult participants (N = 100). These TP subdivisions (dorsal, ventromedial, and ventrolateral) were associated with the information coding of different types/modalities and exhibited specific FC with corresponding neural networks. In Study 2, we demonstrated the presence of the tripartite functional parcellations in the TP of the neonatal brain, based on resting-state FC of dHCP newborns (N = 332, birth age ≤ 4 weeks). Notably, the dorsal and ventrolateral, but not the ventromedial, TP subdivisions in neonates exhibited adult-like specific FC. In Study 3, we observed significant genetic effects for the specific FC of the dorsal and ventrolateral TPs, but not for the ventromedial TP, based on resting-state fMRI images of HCP adult twin participants (N = 380, 123 monozygotic (MZ) and 67 dizygotic (DZ) twin pairs). Importantly, the specific FC between each TP subdivision and each ROI from the corresponding network showed greater heritability for paths present in neonates compared to those absent. In Study 4, we revealed that task-state connectivity patterns of the dorsal and ventrolateral TP subdivisions with their preferred network ROIs could significantly predict these subdivisions' functional activations and participants' behavioral performance during an auditory language comprehension task, based on task-based fMRI data of HCP adult twins (N = 400, 129 MZ and 71 DZ twin pairs). Additionally, the positive associations between neonatal presence and genetic characteristics of the specific FC of TP subdivisions were replicated. Overall, these analyses delineate functional parcellations of the TP with characteristic connections that are present in neonates and genetically regulated during semantic processing in adults. These findings suggest an innate neural topological foundation that facilitates the systematic formation of conceptual knowledge from birth.

Results

Study 1: Tripartite FC-based parcellations in the TP of the adult brain

Functional parcellations of the TP were first characterized in the adult brain using resting-state images of 100 unrelated individuals randomly selected from the HCP database (Table 1). The TP area was delineated using the Harvard-Oxford atlas[35] (probability > 0.2), which relies on anatomical landmarks commonly applied in previous TP parcellation studies[20,21]. A data-driven parcellation approach was applied to divide the left and right TP into distinct subdivisions based on their FC patterns with the rest of the brain (Fig. 1A). Cluster numbers ranging from $k = 2$ to $k = 8$ were computed, and an optimal number of $k = 3$ was chosen for both the left and right TP, which had the highest silhouette values indicating the most efficient segregation (Supplementary Fig. S1). Tripartite functional parcellations within the TP also showed the highest split-half reliability (Dice coefficients for the left TP: 0.91; right TP: 0.92), suggesting optimal reliability and generalizability

Table 1 | Demographic and imaging data characteristics of participants across four studies

	Study 1 (Unrelated adults)	Study 2 (Neonates)	Study 3 (Twin adults)	Study 4 (Twin adults)
Number of participants	100	332	380 (246 MZ and 134 DZ)	400 (258 MZ and 142 DZ)
Age	28.27 ± 3.35 years	1.4 ± 1.09 weeks	29.26 ± 3.38 years	29.22 ± 3.39 years
Sex (female/male)	55/45	146/186	222/158	232/168
fMRI image types	Resting-state	Resting-state	Resting-state	Task-based
Head motion (% of outlier images)	2.74% ± 0.03	4.38% ± 0.03	8.00% ± 0.11	8.53% ± 0.11
Head motion (mean FD after outlier removal, mm)	0.13 ± 0.02	0.10 ± 0.02	0.14 ± 0.02	0.14 ± 0.03

Sex of adults was determined based on self-report, while that of neonates was reported by their parents.
MZ monozygotic, *DZ* dizygotic, *FD* framewise displacement, *mm* millimeter.
Source data are provided as a Source Data file.

https://doi.org/10.1038/s41467-025-58896-y

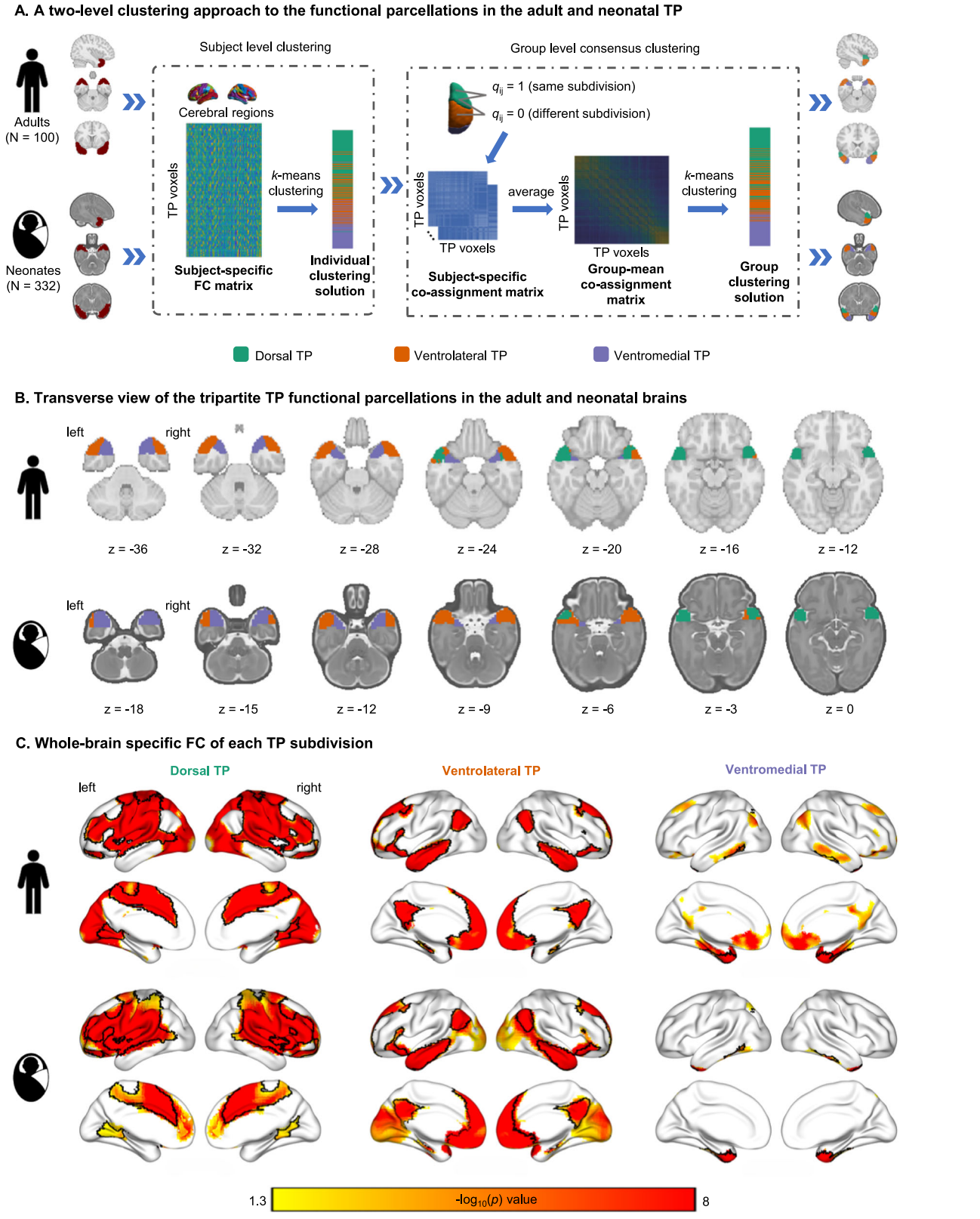

(Supplementary Fig. S2). As shown in Fig. 1B, the TP area in both hemispheres was similarly divided into dorsal, ventrolateral, and ventromedial subdivisions, regardless of whether temporal signal-to-noise ratio (tSNR) effects were controlled (Supplementary Materials).

Our TP subdivisions were consistent with those reported by Pascual and colleagues[21], which were derived from the FC patterns of 40 representative TP seeds and manually adjusted based on cytoarchitectural maps[36]. While our clustering analyses, based on voxel-wise FC patterns without further adjustment, identified three TP subdivisions that were fewer than the four TP parcellations identified by Pascual et al.[21], there was substantial topological overlap between the TP parcellations in both studies. Specifically, our dorsal TP subdivision closely matched that of Pascual et al.[21], and our ventrolateral TP subdivision corresponded entirely with their anterolateral TP

Fig. 1 | Tripartite functional parcellations in the temporal pole (TP) detected in adult and neonatal brains. A Flowchart of the two-level clustering approach used to parcellate the TP areas based on their whole-brain functional connectivity (FC) patterns in both the adult and neonatal (birth age ≤ 4 weeks) brains. For each adult participant, an FC matrix was computed between TP voxels and AAL-defined cerebral regions across the whole brain. This matrix was then subjected to K-means clustering to generate subject-specific TP parcellation maps. A co-assignment matrix, indicating whether pairs of TP voxels were assigned to the same subdivision (1 = yes, 0 = no), was computed for each participant. These matrices were averaged across all adult participants to create a group-level co-assignment matrix. A second K-means clustering analysis was applied to this group-level matrix, resulting in a final group-level TP parcellation map for the adult brain. The same procedure was applied to neonatal fMRI data, producing functional parcellations within the neonatal TP area. **B** Transverse views of the tripartite functional parcellations in adult and neonatal TPs from bottom slices (left) to top slices (right). **C** Whole-brain specific FC maps for each TP subdivision in both adult and neonatal brains. These maps were generated by comparing the FC maps of one subdivision (e.g., dorsal TP) with the mean FC maps of the other two subdivisions (e.g., ventrolateral TP and ventromedial TP) using paired *t*-tests (one-tailed, $p < 0.05$, FDR corrected, cluster size > 50 voxels). The overlapping areas in the FC maps of the same TP subdivision between adult and neonatal participants are outlined in black. AAL: Anatomical Automatic Labeling atlas.

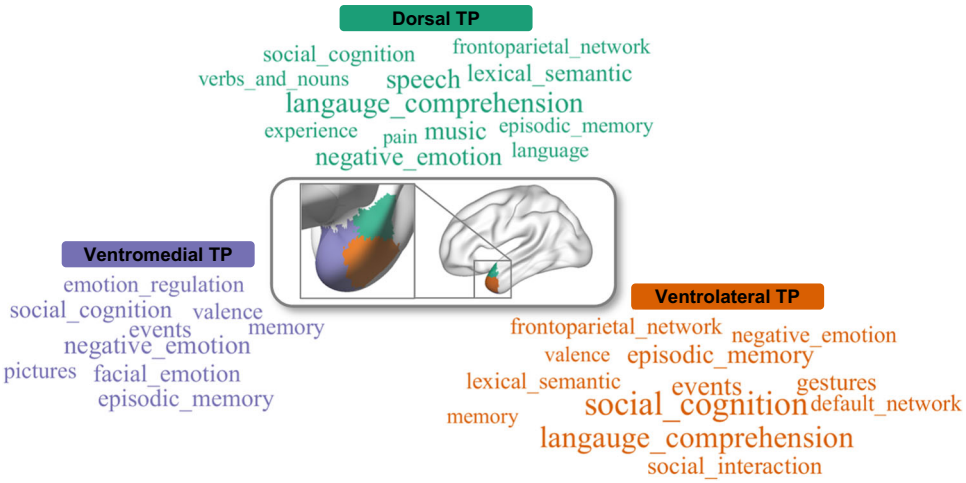

Fig. 2 | Distinctive functional preferences of the three temporal pole (TP) subdivisions revealed by Neurosynth-based meta-analyses. Word clouds indicate research topics that are significantly associated with functional activations in each TP subdivision, with font size varying according to the degree of association ($p < 0.05$, FDR corrected, two-tailed).

region. Our study delineated a relatively larger ventromedial TP subdivision, which encompassed both the ventromedial and medial regions identified by Pascual et al.[21] and extended into their anterolateral TP region. Notably, by combining the ventromedial and medial regions from Pascual et al.'s study into one cluster, we found that 82.5% of their TP seeds were classified into the same subdivision in our analyses, highlighting the consistency of findings across studies (see comparisons of TP parcellations across studies in Supplementary Table S1).

To characterize the specific FC of the TP subdivisions, we conducted paired *t*-tests to compare the whole-brain FC maps of one subdivision (e.g., left dorsal TP) with the mean FC maps of the other two subdivisions in the same hemisphere (e.g., left ventrolateral TP and ventromedial TP; significance threshold: voxel-level $p < 0.05$, FDR corrected, cluster size ≥ 50 voxels). Replicating previous studies[20,24], we observed highly similar FC patterns for the same TP subdivision across both hemispheres (Supplementary Fig. S4), which were thus combined into one bilateral subdivision for subsequent analyses. Different TP subdivisions exhibited preferential connectivity with distinct brain regions, a pattern consistent with previous findings[20,21] (Fig. 1C). Specifically, the dorsal TP showed greater connectivity with large-scale bilateral primary auditory and adjacent areas, the frontotemporal language areas, and motor/somatosensory cortices. The specific FC of the dorsal TP also extended to multimodal semantic processing regions, including the inferior frontal and lateral posterior temporal cortices (see similar results in ref. 25). The ventrolateral TP showed stronger bilateral FC with the middle temporal gyri, angular gyri, dorsolateral and ventrolateral prefrontal gyri, insula, and anterior/posterior cingulate areas. These regions are generally considered to compose the default mode network[37–39], while some of the identified regions, including the angular, ventrolateral prefrontal and middle temporal gyri, also play key roles in general semantic processing[13,40]. The ventromedial TP exhibited greater FC with higher-order ventral temporal visual areas (i.e., the middle and anterior parts of the inferior temporal, fusiform, and parahippocampal gyri), middle frontal gyri, and the paralimbic system, including the olfactory cortex and ventral orbitofrontal cortex.

To objectively examine the generic functional preferences of each TP subdivision, we conducted large-scale meta-analyses using the Neurosynth database, which comprises 14371 fMRI studies and over 150000 activation peaks[41] (version 0.7, released July 2018). Our analyses focused on 67 cognition-related research topics that encompass all mental processes involved in knowledge acquisition, information manipulation, and reasoning, such as perception, memory, attention, and language[42] (Supplementary Table S2). The results revealed 21 research topics that were significantly associated with functional activations in the TP ($p_{FDR\text{-}corrected} < 0.05$), with distinct association patterns across the three TP subdivisions (Fig. 2 and Supplementary Table S2). While shared associations were found for the topics of episodic memory, negative emotion, and social cognition, the dorsal TP showed unique associations with language, speech, verbs and nouns, music, experience, and pain, most of which were auditory or language related. The ventromedial TP was specifically linked to visual or emotion-related topics, including facial emotion, pictures and emotion regulation. The ventrolateral TP was associated with a broader range of topics; in addition to unique associations with the default network, gestures and social interaction, it also had shared associations with the dorsal (lexical semantics, language comprehension and frontoparietal network) and the ventromedial (valence, events and memory) TP subdivisions. Overall, while shared cognitive functions were evident in the TP, the

functional parcellations of the TP exhibited distinct functional preferences in processing information of different types/modalities, aligning well with the preferential connectivity patterns of each TP subdivision. Specifically, the dorsal-to-ventral transition from auditory/language to visual/emotional information processing in the TP is consistent with the specific FC of the dorsal TP with the auditory and language areas, and the ventromedial TP with the visual pathway and the paralimbic system, which plays a crucial role in emotional processing[43,44]. The broader involvement of the ventrolateral TP in diverse and multimodal information processing also aligns with its predominant connections with the default and semantic networks.

Subsequently, we conducted ROI analyses to validate the specific FC of TP subdivisions with the corresponding neural networks defined based on meta-analyses and anatomical landmarks (Fig. 3A, *Network ROI selection*). These networks were the auditory language network (for the dorsal TP), the visual paralimbic network (for the ventromedial TP) and the default semantic network (for the ventrolateral TP). We named these networks following the network labels used in Pascual et al.[21] given the consistent TP parcellations and the associated FC results observed in both their study and ours. Note that the auditory language network associated with the dorsal TP was slightly different from that in Pascual et al.[21] ("somatosensory auditory network"), to reflect the significant overlap between the whole-brain FC results of the dorsal TP and language processing regions observed in our study (also noted by refs. 20, 21). The FC strength between each TP subdivision and each neural network was computed (see *Network ROI selection*) and submitted to ANOVA analyses to determine whether the FC strength of the three TP subdivisions with each network differed significantly. The results revealed a significant main effect of TP subdivision on the auditory language ($F_{(2,\ 198)} = 150.66$, $p < 0.001$, *partial* $\eta^2 = 0.60$), default semantic ($F_{(2,\ 198)} = 345.51$, $p < 0.001$, *partial* $\eta^2 = 0.78$), and visual paralimbic ($F_{(2,\ 198)} = 10.94$, $p < 0.001$, *partial* $\eta^2 = 0.10$) networks. Pairwise comparisons performed to examine the putative specific FC of each TP subdivision with the corresponding network showed that the dorsal TP exhibited greater FC strength with the auditory language network than did the ventrolateral ($t_{99} = 5.23$, $p_{corrected} < 0.001$, FWE-corrected, *Cohen's d* = 0.52, 95% CI = [0.037, 0.081]) and ventromedial ($t_{99} = 15.82$, $p_{corrected} < 0.001$, *Cohen's d* = 1.58, 95% CI = [0.15, 0.19]) TP subdivisions (Fig. 3B). Similarly, the ventrolateral TP was more strongly connected with the default semantic network than the ventromedial TP ($t_{99} = 15.32$, $p_{corrected} < 0.001$, *Cohen's d* = 1.53, 95% CI = [0.13, 0.17]) and dorsal TP ($t_{99} = 24.08$, $p_{corrected} < 0.001$, *Cohen's d* = 2.41, 95% CI = [0.32, 0.38]). Lastly, the ventromedial TP was more strongly linked to the visual paralimbic network than both the dorsal TP ($t_{99} = 3.30$, $p_{corrected} = 0.003$, *Cohen's d* = 0.33, 95% CI = [0.012, 0.047]) and ventrolateral TP ($t_{99} = 5.85$, $p_{corrected} < 0.001$, *Cohen's d* = 0.59, 95% CI = [0.023, 0.046]). Notably, the specific FC strength of different TP subdivisions was also observable at the network node level, where 19 out of 23 network ROIs demonstrated greater FC strength with their respective TP subdivision than the mean FC strength with the other two subdivisions (Fig. 3B, all $p_{corrected} < 0.05$).

In summary, we identified tripartite functional parcellations of the TP in the adult brain that were consistent with previous TP parcellation work[20–22]. These TP subdivisions exhibited distinct functional preferences for information processing of different types/modalities, and showed specific FC with corresponding neural networks. These findings lend support to neural semantic frameworks that propose functional heterogeneity in the TP for multimodal conceptual representation[9,12,23,27].

Study 2: Neonatal presence of TP parcellations exhibiting specific FC with semantic-related networks

Functional parcellations of the TP in the neonatal brain were characterized using the same clustering techniques on resting-state images of 332 newborns (birth age ≤ 4 weeks, birth age = 1.40 ± 1.09 weeks, gestational age = 40.10 ± 2.97 weeks, Table 1) available from the dHCP database (third release). The left and right TP areas generated in the adult space were warped onto the 40-week templates available on the dHCP website (https://git.fmrib.ox.ac.uk/seanf/dhcp-resources/-/blob/master/docs/dhcp-augmented-volumetric-atlas-extended.md#download-42-gb) using Advanced Normalization Tools[45]. The TP areas in both hemispheres of the neonatal brain were parcellated using the same number of parcellations, $k = 3$, as applied for the adults, given the goal of the current study to examine the early precursors of the functional divisions of the TP observed in the mature brain. Similar to those in adults, clustering analyses in neonates revealed highly symmetric dorsal, ventrolateral and ventromedial subdivisions in the left and right TP (Fig. 1B). Overlapping analyses quantifying the topological similarities between the TP subdivisions in the adult and neonatal brains showed high Dice coefficients for both the overall parcellations (left: 0.73; right: 0.75) and the individual subdivisions (left: dorsal: 0.81; ventrolateral: 0.67; ventromedial: 0.73; right: dorsal: 0.76; ventrolateral: 0.69; ventromedial: 0.81. See Supplementary Fig. S5 for the complete parcellation results of the neonatal TP for the cluster numbers ranging from $k = 2$ to $k = 8$).

Paired *t*-tests were performed to identify the specific FC map of each TP subdivision in neonates. Again, highly similar FC patterns were revealed for the same TP subdivision in both hemispheres, which were combined for further analyses (Supplementary Fig. S4). The specific FC maps of the bilateral dorsal and ventrolateral TP subdivisions in neonates largely overlapped with those observed in adults (Fig. 1C). The dorsal TP exhibited stronger connectivity with auditory, language, and somatosensory regions, while the ventrolateral TP was primarily connected with regions of the default semantic network. However, some differences in FC patterns were noted between neonates and adults. The dorsal TP in neonates showed less FC with the posterior temporal and occipital cortices compared to adults. The most pronounced contrast was observed in the specific FC map of the ventromedial TP. Unlike the preferred FC of the ventromedial TP with higher-order visual pathways and paralimbic systems in the adult brain, the neonatal ventromedial TP exhibited very limited specific FC across the whole brain, primarily restricted to the ventral temporal visual areas.

The ROI results further confirmed the adult-like specific connections of the dorsal and ventrolateral TP subdivisions in the neonatal brain. Using the same network ROIs (warped to the neonatal spaces using ANTs), ANOVAs revealed significant differences in the FC strength of the three TP subdivisions with the auditory language ($F_{(2,\ 662)} = 393.69$, $p < 0.001$, *partial* $\eta^2 = 0.54$), default semantic ($F_{(2,\ 662)} = 90.20$, $p < 0.001$, *partial* $\eta^2 = 0.21$), and visual paralimbic ($F_{(2,\ 662)} = 15.53$, $p < 0.001$, *partial* $\eta^2 = 0.05$) networks. Importantly, planned pairwise comparisons aimed at assessing the adult-like predominant FC of each TP subdivision in neonates revealed stronger FC strength between the auditory language network and the dorsal TP than with the ventrolateral ($t_{331} = 14.93$, $p_{corrected} < 0.001$, one-tailed, *Cohen's d* = 0.82, 95% CI = [0.097, 0.13]) and ventromedial ($t_{331} = 23.85$, $p_{corrected} < 0.001$, one-tailed, *Cohen's d* = 1.31, 95% CI = [0.20, 0.23]) TP subdivisions, as well as greater FC strength between the default semantic network and the ventrolateral TP than with the dorsal ($t_{331} = 8.61$, $p_{corrected} < 0.001$, one-tailed, *Cohen's d* = 0.47, 95% CI = [0.051, 0.081]) and ventromedial ($t_{331} = 16.34$, $p_{corrected} < 0.001$, one-tailed, *Cohen's d* = 0.90, 95% CI = [0.094, 0.12]) TP subdivisions (Fig. 3C). In contrast, the neonatal ventromedial TP failed to establish stronger adult-like FC with the visual paralimbic network than did the dorsal and ventrolateral TP subdivisions (both $p > 0.20$, one-tailed). This pattern was also evident at the network node level: while all default semantic and auditory language network ROIs (except for the left and right occipital gyri) showed stronger FC strength with their respective TP subdivision than the mean FC strength with the other two subdivisions (all $p_{corrected} < 0.05$,

https://doi.org/10.1038/s41467-025-58896-y

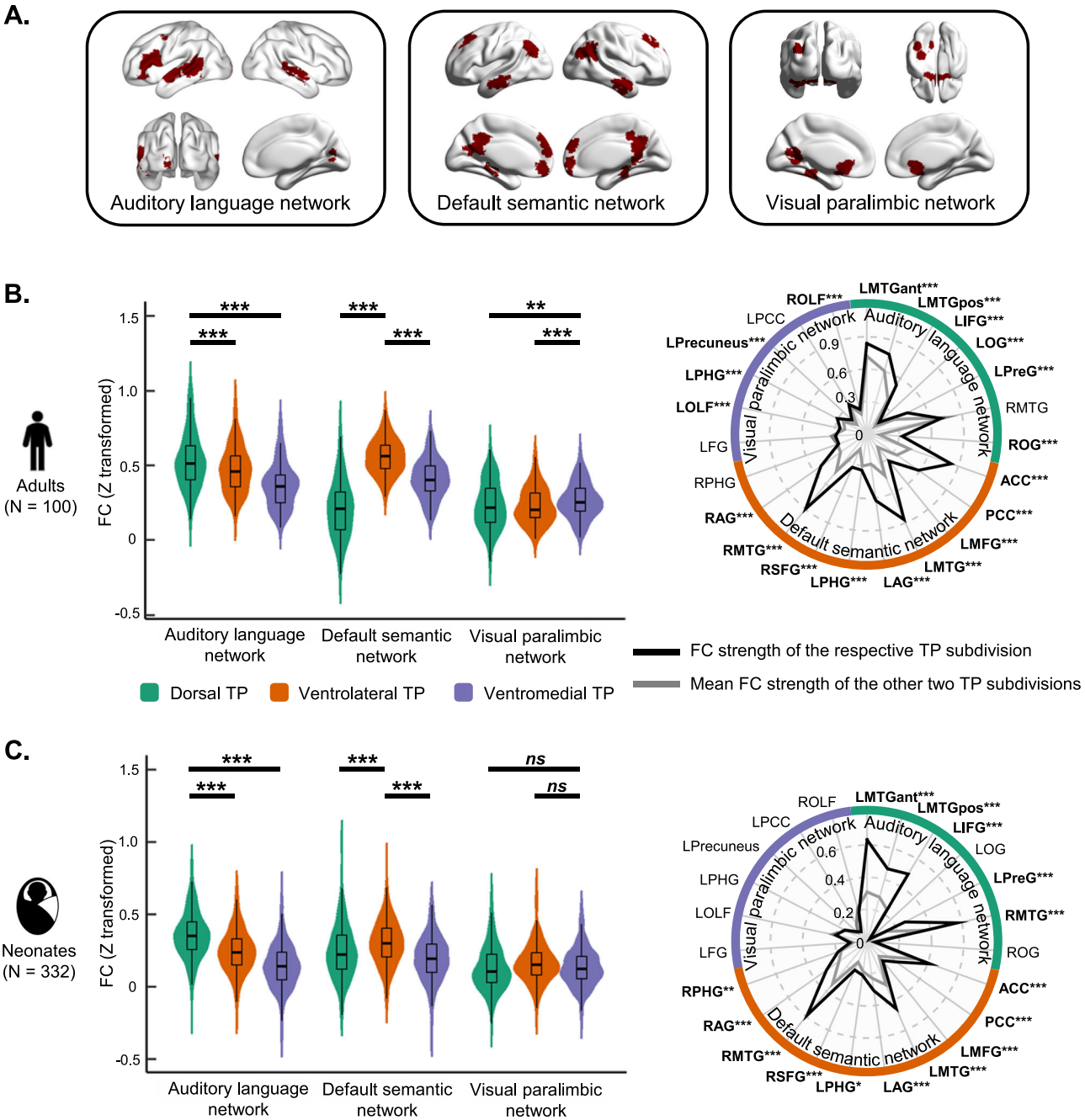

Fig. 3 | Specific functional connectivity (FC) of the temporal pole (TP) subdivisions in adult and neonatal brains revealed by region of interest (ROI) analyses. A Brain images illustrating the auditory language network, the default semantic network, and the visual paralimbic network, which were used in the ROI analyses (see Methods: *Network ROI selection*). **B**, **C** Specific FC of each TP subdivision in the adult (**B**) and neonatal (**C**) brains. The violin plots (left) display the data density of FC strength between each TP subdivision and each neural network. The boxplots indicate the 25th and 75th percentiles (lower and upper hinges) and the median (middle line), while the whiskers extend to values within 1.5 × the interquartile range (IQR). Differences between the FC strength of each TP subdivision with the corresponding neural network and that of the other subdivisions with the same neural network were examined using *t*-tests (two-tailed for adults, one-tailed for neonates, FWE corrected; detailed *p* values are provided in Source Data file). The radar plots (right) illustrate FC comparisons between the respective TP subdivision and the mean FC strength of the other two subdivisions for each network node (*t*-test, one-tailed, FWE corrected; detailed *p* values are provided in Source Data file). AAL: Anatomical Automatic Labeling atlas. Auditory language network ROIs: LMTGant, left anterior middle temporal gyrus; LMTGpos, left posterior middle temporal gyrus; LIFG, left inferior frontal gyrus; LOG, left occipital gyrus; LPreG, left precentral gyrus; RMTG, right middle temporal gyrus; ROG, right occipital gyrus. Default semantic network ROIs: LMTG, left middle temporal gyrus; RMTG, right middle temporal gyrus; LPHG, left parahippocampal gyrus; RPHG, right parahippocampal gyrus; LAG, left angular gyrus; RAG, right angular gyrus; LMFG, left middle frontal gyrus, RSFG, right superior frontal gyrus, ACC, anterior cingulate cortex; PCC, posterior cingulate cortex. Visual paralimbic network ROIs: LPrecuneus, left precuneus gyrus, LPCC, left posterior cingulate cortex, LFG, left fusiform gyrus; LPHG, left parahippocampal gyrus; LOLF, left olfactory cortex; ROLF, right olfactory cortex. *** $p_{FWE\text{-}corrected} < 0.001$, ** $p_{FWE\text{-}corrected} < 0.01$, * $p_{FWE\text{-}corrected} < 0.05$, *ns*, not significant. Source data are provided as a Source Data file.

https://doi.org/10.1038/s41467-025-58896-y

one-tailed), none of the ROIs from the visual paralimbic network were more strongly connected to the ventromedial TP than to the other two subdivisions (Fig. 3C).

Overall, the current study provides empirical evidence for the early emergence of adult-like functional parcellations of the TP in the neonatal brain. Moreover, the specific functional connectivity of the dorsal and ventrolateral TP subdivisions with the auditory language and default semantic networks, respectively, corresponded well with the FC and functional preference characteristics of the same TP subdivisions in adults (see Supplementary Fig. S3 for consistent result patterns after controlling for the tSNR). These similarities suggest the early presence of connectivity-based functional parcellations in the TP that may support its putative role in conceptual representation with early-established contributions from auditory/linguistic experiences.

Study 3: Genetic bases of the specific FC of TP subdivisions in twin adults at rest

Given the presence of TP parcellations with specialized connections with the auditory language (dorsal TP) and default semantic (ventrolateral TP) networks in newborns with limited environmental influences, we hypothesized significant genetic contributions to these specific connections. These genetic influences might manifest in the heritable characteristics of individual differences observed in adults. These hypotheses were examined using the resting-state images of adult twin participants from the HCP dataset (N = 380, 246 MZ and 134 DZ twins, Table 1). Utilizing network ROIs created in Study 1, the specific FC of each TP subdivision with the corresponding network was calculated as the difference between the FC strength of one TP subdivision with its preferred network and the mean FC strength of the other subdivisions with the same network (e.g., specific FC of dorsal TP = FC $\text{strength}_{\text{dorsal TP-auditory language}}$ − (FC $\text{strength}_{\text{ventrolateral TP-auditory language}}$ + FC $\text{strength}_{\text{ventromedial TP-auditory language}}$)/2) for every participant. We employed univariate structural equation models (SEM) to statistically examine the genetic contributions to the specific FC of the TP subdivisions. These models decomposed the observed cross-participant covariances of the phenotype of interest (the specific FC of each TP subdivision in this case) into additive genetic (A), common environmental (C) and unique environmental (E, including measurement errors) factors. Age and sex were included as covariates. Model-fitting analyses demonstrated that the data for the dorsal and ventrolateral TP subdivisions were best explained by a model incorporating the additive genetic and unique environmental factors (i.e., an AE model, Table 2). These results indicated significant genetic contributions to the individual variability in the specific FC of these two TP subdivisions (dorsal: $a^2 = 0.36$, $p < 0.001$, 95% CI = [0.35, 0.37]; ventrolateral: $a^2 = 0.46$, $p < 0.001$, 95% CI = [0.45, 0.48]). In contrast, the best-fit model for the specific FC of the ventromedial TP included common and unique environmental factors (i.e., CE model), suggesting significant common environmental effects ($c^2 = 0.23$, $p = 0.002$, 95% CI = [0.22, 0.24]; Table 2). Permutation analyses based on full ACE models with shuffled MZ and DZ labels and randomized twin pairs (N = 10000) confirmed the identified significant effects of additive genetics or the common environmental factors for each TP subdivision (all $p_{\text{permutation}} < 0.05$). Moreover, these analyses revealed significantly greater additive genetic contributions compared to those of the common environmental factors for the ventrolateral TP ($p_{\text{permutation}} < 0.001$), but no significant differences between the two factors for the dorsal ($p_{\text{permutation}} = 0.28$) and ventromedial ($p_{\text{permutation}} = 0.09$) TP subdivisions.

The twin-based study revealed significant heritability in the individual differences in the specific FC of the dorsal and ventrolateral TP subdivisions that were observable shortly after birth, suggesting potential associations between the early emergence and genetic mechanisms of the characteristic functional connections of TP parcellations. To further test this relationship at a finer scale, we

Table 2 | Optimal models for univariate structural equation modeling of the specific FC of TP subdivisions and behavioral performance during an auditory language comprehension task in twin adults

	Intraclass correlation		Best fit model	AIC	a^2 (95% CI)	c^2 (95% CI)	e^2 (95% CI)	p
	MZ (p)	DZ (p)						
Resting-state FC								
Dorsal TP with the auditory language network	0.40 (2.80E-06)	0.31 (0.005)	AE	-1473.79	0.36 (0.35–0.37)	-	0.64 (0.63–0.65)	4.82E-06
Ventrolateral TP with the default semantic network	0.49 (5.40E-09)	0.18 (0.075)	AE	-1411.94	0.46 (0.45–0.48)	-	0.54 (0.53–0.54)	1.2E-08
Ventromedial TP with the visual paralimbic network	0.24 (0.003)	0.20 (0.051)	CE	-1796.48	-	0.23 (0.22–0.24)	0.77 (0.77–0.78)	0.002
Task-based FC								
Dorsal TP with the auditory language network	0.17 (0.029)	0.12 (0.16)	AE	-1347.98	0.17 (0.15–0.19)	-	0.83 (0.82–0.84)	0.034
Ventrolateral TP with the default semantic network	0.17 (0.024)	0.06 (0.30)	AE	-1466.69	0.16 (0.14–0.18)	-	0.84 (0.83–0.85)	0.049
Ventromedial TP with the visual paralimbic network	0.03 (0.35)	0.15 (0.10)	E	-1499.62	-	-	1.00 (1.00–1.00)	-
Task performance								
Task difficulty level	0.44 (1.52E-07)	0.22 (0.07)	AE	567.11	0.41 (0.23–0.59)	-	0.59 (0.47–0.71)	5.15E-07

Both the full ACE model and the submodels (AE, CE and E models) were examined for the specific functional connectivity (FC) of each temporal pole (TP) subdivision. The best fit model was selected based on the Akaike information criterion (AIC), which takes both model parsimony and goodness of fit into consideration. Moreover, when an AE or CE model was selected, the significance (p) of the additive genetic (a^2) or common environmental (c^2) effects was estimated by comparison to the E model using χ^2 tests (one-tailed).
MZ monozygotic, *DZ* dizygotic, *A* additive genetic factors, *C* common environmental factors, *E* unique environmental factors and measurement errors, *CI* confidence interval.

https://doi.org/10.1038/s41467-025-58896-y

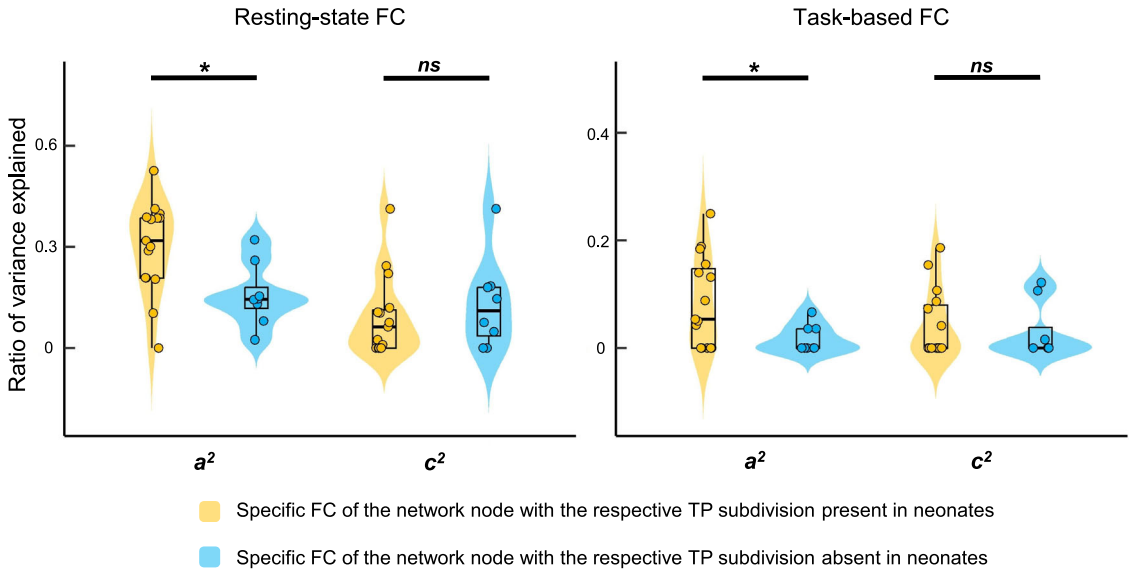

Fig. 4 | Associations between neonatal and genetic characteristics of the specific functional connectivity (FC) of temporal pole (TP) subdivisions with the corresponding network nodes (i.e., regions of interest, N = 23). The violin plots illustrate the data density of the additive genetic (a^2) and common environmental (c^2) effects on the specific FC of TP subdivisions with the corresponding network nodes. These effects were estimated using the full ACE model in the structural equation modeling analyses, based on FC during both the resting-state and auditory language comprehension conditions. Nodes from the three networks were categorized into two groups based on whether the specific FC of a node with its respective TP subdivision was established in the neonatal brain (as shown in the node-specific results in the radar graph in Fig. 3C). Two-sample *t*-tests were performed to compare the genetic and environmental effects between the connections of these two types of nodes (two-tailed). The boxplots indicate the 25th and 75th percentiles (lower and upper hinges) and the median (middle line), while the whiskers extend to values within 1.5 × IQR. * $p < 0.05$, *ns*, not significant. Source data are provided as a Source Data file.

categorized all nodes (ROIs) from the three networks into two groups based on whether the specific FC of a node with its respective TP subdivision was established in the neonatal brain (e.g., a language network node showing greater FC strength with the dorsal TP than the mean FC strength with the other two TP subdivisions, $p_{corrected} < 0.05$, Fig. 3C). Moreover, the additive genetic (a^2) and common environmental (c^2) effects were estimated for the specific FC associated with each node using the full ACE models in the SEM analyses. Two-sample *t*-tests revealed significantly greater a^2 values for the nodes that showed specific FC in neonates than for the nodes that did not ($t_{21} = 2.65$, $p = 0.015$, *Cohen's d* = 1.16, 95% CI = [0.031, 0.26]; Fig. 4), revealing node-level associations between the inborn and genetic characteristics of the specific FC of the TP subdivisions. No significant group differences were found for the common environmental effects ($t_{21} = -0.71$, $p = 0.49$; Fig. 4).

To summarize, by combining neonate- and twin-based imaging analyses, we demonstrated significant genetic contributions to adult variations in specific functional connections between TP subdivisions and the auditory language (dorsal TP) and default semantic (ventrolateral TP) networks that were present in neonates. These results suggest early-emerging and enduring genetic control over the connection characteristics of TP subdivisions with neural networks for information processing, especially auditory/linguistic related.

Study 4: Genetic bases of the specific FC of TP subdivisions in association with semantic processing in twin adults

Building on the early emerging and genetically controlled FC of the dorsal and ventrolateral TP subdivisions with the auditory language and default semantic networks, we explored their functional relevance in semantic processing using task-based fMRI data of HCP twin participants (N = 400, 258 MZ and 142 DZ twins, Table 1). Functional MRI images were collected during an auditory story comprehension task adapted from Binder et al.[46]. In this task, participants listened to eight blocks of brief auditory stories (5–9 sentences) adapted from Aesop's fables and answered a two-choice comprehension question at the end of each block. Multiple difficulty levels were created by manipulating the vocabulary complexity of the stories and the semantic relatedness of the probe choices. To maintain participants' attention, the difficulty level was adjusted dynamically based on their ongoing performance; it increased after correct responses and decreased following incorrect responses. A math task assessing arithmetic skills was also included in separate blocks within the same experiment, which involved solving addition and subtraction problems tailored to individual performance levels. Traditional univariate analyses revealed significantly greater activation in classic language areas during the auditory language comprehension task compared to baseline[47,48], i.e., the fixation period, Fig. 5A and Supplementary Table S3), which largely overlapped with the predefined auditory language network (77% of activated voxels) but minimally overlapped with the default semantic (7%) and visual paralimbic networks (0%). Task-induced activations also extended into the dorsal (75%) and ventrolateral (81%) TP subdivisions but largely avoided the ventromedial TP (24%), suggesting relatively selective engagement of TP subdivisions in auditory language processing. In contrast, the math condition activated most of the math-related areas (Supplementary Fig. S6A and Table S3), including the bilateral middle and superior frontal, inferior parietal and superior temporal gyri. These regions overlapped with parts of the auditory language network (39%), likely due to the shared input modality, but involved little of the default semantic (0%) and visual paralimbic (7%) networks. The TP areas were minimally involved during the math task (dorsal TP: 22%, ventrolateral TP: 0%, ventromedial TP: 0%), indicating a lack of functional relevance for arithmetic processing.

We first conducted the genetic-based analyses on the specific FC of TP subdivisions using FC measures under the auditory language comprehension condition. Similar to results based on resting-state FC measurements, SEM analyses revealed that the AE model was the best-fit model for both the dorsal and ventrolateral TP subdivisions with significant genetic effects (dorsal TP: $a^2 = 0.17$, $p = 0.034$, 95% CI = [0.15, 0.19]; ventrolateral TP: $a^2 = 0.16$, $p = 0.049$, 95% CI = [0.14, 0.18]),

https://doi.org/10.1038/s41467-025-58896-y

A. Whole-brain results for the auditory language comprehension task compared to baseline.

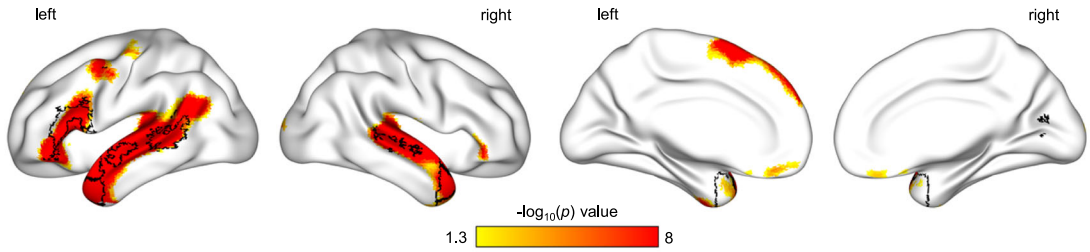

B. Association results of the connection characteristics of TP subdivisions with functional activations and task performance during the auditory language comprehension task.

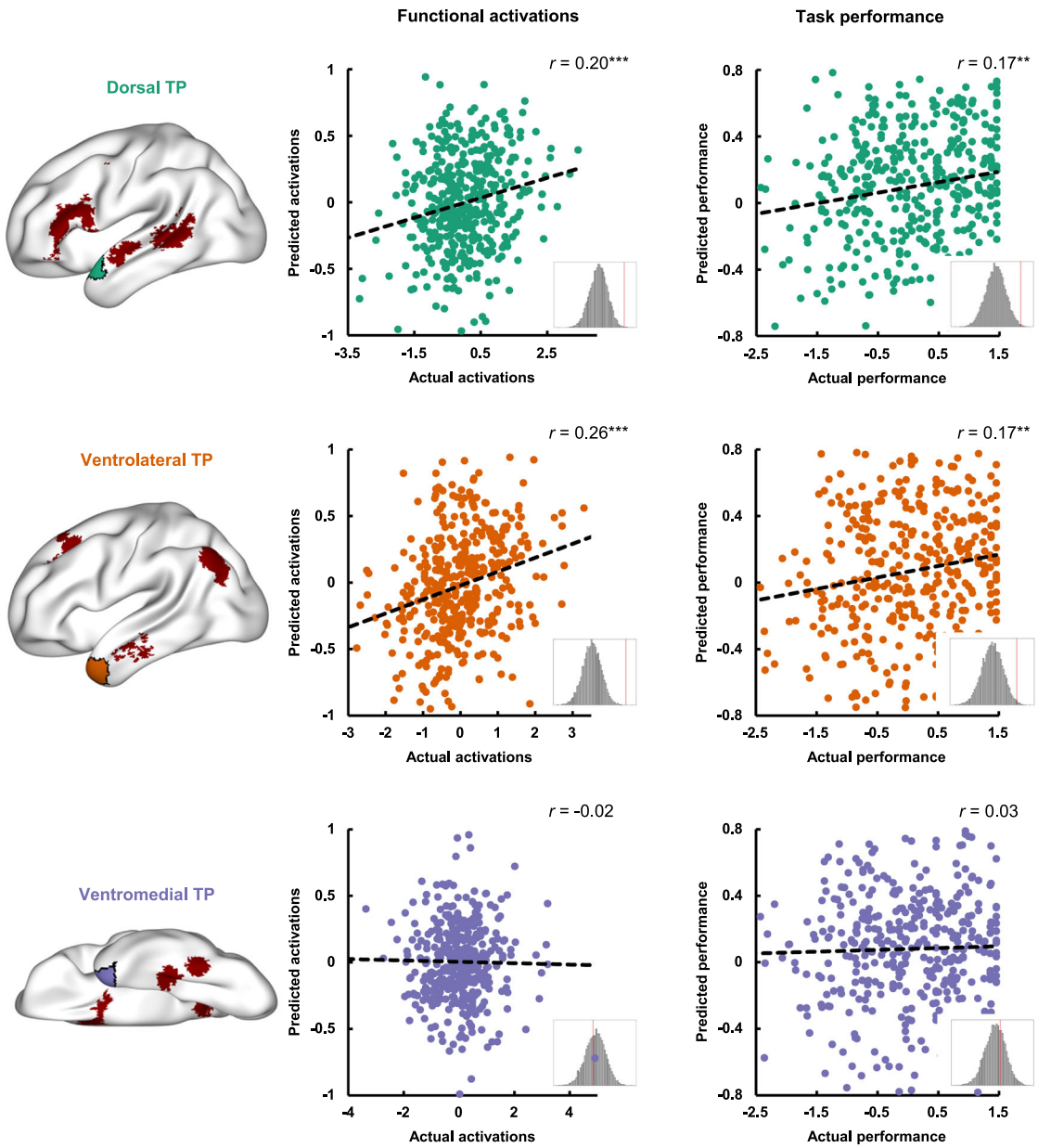

whereas the E model with only the unique environmental factor was selected as the optimal model for the ventromedial TP (Table 2). Permutation analyses confirmed the identified significant additive genetic effects for the dorsal and ventrolateral TP subdivisions (both $p_{permutation} < 0.05$) but not for the ventromedial TP ($p_{permutation} = 0.69$). Moreover, these analyses revealed significantly greater additive genetic contributions compared to those of the common environmental factors for the dorsal ($p_{permutation} = 0.008$) and ventrolateral TP ($p_{permutation} = 0.007$) subdivisions but not for the ventromedial TP ($p_{permutation} = 0.96$). In addition, we replicated the node-level associations between neonatal presence and genetic effects of the specific FC of TP subdivisions, where significantly greater additive genetic effects were observed for the specific FC of network nodes with the respective TP subdivisions that were present in

Fig. 5 | The connection characteristics of the dorsal and ventrolateral temporal pole (TP) subdivisions, but not the ventromedial TP subdivision, significantly predicted both functional activations of the same TP subdivision and behavioral performance during the auditory language comprehension task in adult twins (N = 400). A Brain figures illustrating whole-brain activations during the language comprehension task compared to baseline (i.e., the fixation period; *t*-test, one-tailed, voxel level $p < 0.05$, FDR corrected, cluster size > 50 voxels). The auditory language network and TP area are outlined in black. **B** Scatter plots showing the association results of the FC matrices between each TP subdivision and its preferred network ROIs (illustrated in the brain figure next to the y-axis) for the functional responses of this TP subdivision (left column) and behavioral performance (right column) during auditory language comprehension. The significance of support vector regression performance was assessed using the null distribution (bottom right corner) generated from permutation tests ($n = 10000$). *** $p_{permutation} < 0.001$, ** $p_{permutation} < 0.01$. Source data are provided as a Source Data file.

neonates compared to those that were absent ($t_{21} = 2.24$, $p = 0.036$, *Cohen's d* = 0.98, 95% CI = [0.005, 0.13]), whereas no differences in common environmental effects ($t_{21} = 0.49$, $p = 0.63$, Fig. 4) were revealed.

Using support vector regression (SVR) models, we evaluated the associations between the connection characteristics of TP subdivisions with the corresponding network and their functional activations during auditory language comprehension and math computation tasks. Given the optimal performance of using multivariate characteristics of connectivity patterns from one region to predict its functional relevance[49–51], we employed FC matrices of each TP subdivision with the ROIs from the corresponding network in these analyses. For instance, for the dorsal TP, a 400 × 7 (participants × language ROIs) data matrix served as input features for the SVR models. These models were trained to predict the functional activations of the same TP subdivision during the language comprehension task using the LIBSVM package[52]. Prediction performance was evaluated through cross-validation. The results demonstrated that the semantically related functional activations of the dorsal and ventrolateral TP subdivisions could be significantly predicted by their concurrent FC patterns with the corresponding network ROIs (dorsal TP with the auditory language network ROIs: $r = 0.20$, $p_{permutation} = 0.001$, 95% CI = [0.11, 0.29]; ventrolateral TP with the default semantic network ROIs: $r = 0.26$, $p_{permutation} < 0.001$, 95% CI = [0.17, 0.35]; Fig. 5B), whereas the associations between the functional activations of the ventromedial TP and its FC patterns with the visual paralimbic network ROIs were not significant ($r = -0.02$, $p_{permutation} = 0.60$, Fig. 5B). Furthermore, no significant associations were found between the functional activations of the three TP subdivisions during the math task and their FC matrices with the corresponding network ROIs under the same condition (all $p_{permutation} > 0.07$, Supplementary Fig. S6B–D).

To link neural network characteristics to behavior, we further conducted SVR analyses to assess whether the FC pattern of TP subdivisions were associated with participants' behavioral performance on this auditory language comprehension task. Due to the administration of various stimuli to different participants, task accuracies and response times were not directly comparable. We utilized task difficulty levels available in the HCP database as a proxy for each participant's overall language comprehension abilities (mean = 10.5 ± 1.4, range = 4.9-12.6, with higher values indicating better performance; see similar methodologies in refs. 46,53). Genetic-based analyses (i.e., univariate SEM) revealed significant heritable patterns in individual differences in task difficulty levels ($a^2 = 0.41$, $p < 0.001$, 95% CI = [0.23, 0.59]), with the AE model as the best-fit model (Table 2). Using individual task difficulty levels as outcome measures, SVR analyses identified significant associations between this behavioral measure and the FC matrices of the dorsal ($r = 0.17$, $p_{permutation} = 0.004$, 95% CI = [0.078, 0.27]) and ventrolateral ($r = 0.17$, $p_{permutation} = 0.007$, 95% CI = [0.069, 0.26], Fig. 5B) TP subdivisions. No significant association was found for the FC patterns of the ventromedial TP subdivisions ($r = 0.03$, $p_{permutation} = 0.32$, Fig. 5B). These significant associations at both the brain (functional activations) and behavioral (task difficulty) levels collectively suggest specific links between the connection characteristics of the dorsal and ventrolateral TP subdivisions and their functional roles in semantic processing during the auditory language comprehension task.

In summary, analyses based on task-based fMRI data of twin adults revealed significant and dominant heritable patterns in the specific FC that were neonatally established between the dorsal TP and the auditory language network and between the ventrolateral TP and the default semantic network, replicating findings derived from resting-state FC patterns. Importantly, we demonstrated that the connection characteristics of the dorsal and ventrolateral TP subdivisions significantly predicted both the functional activations and participants' behavioral performance during an auditory language comprehension task. This underscores the functional significance of these early emerging and genetically controlled network characteristics of TP subdivisions in semantic processing.

Discussion

In the current study, we combined neonatal and twin-based imaging analyses to reveal the developmental origins of the semantic system in the human brain. Focusing on the temporal pole, a putative hub for semantic processing identified in adult research, we revealed tripartite functional parcellations within the adult TP, each associated with distinct neural networks (Study 1). These TP subdivisions, with specific FC of the dorsal and ventrolateral TP, were observable in neonates within their first month of life (Study 2), and exhibited significant heritable patterns in adult twins both at rest (Study 3) and during an auditory language comprehension task (Study 4). Furthermore, the FC patterns of the dorsal and ventrolateral TP with their respective networks significantly predicted participants' behavioral performance and the neural responses of the same TP subdivisions during the comprehension task, highlighting their functional significance in semantic processing (Study 4). Collectively, our findings advance the understanding of the neurodevelopmental precursors of semantic cognition by delineating the neonatally established and genetically influenced network characteristics of TP subdivisions in association with their functional roles in adult semantic cognition (Fig. 6).

The observation of TP parcellations in the adult brain supports the notion of graded functions within the TP for its putative hub role in the neural semantic representation of humans[12]. Our FC-based clustering method identified highly symmetric TP subdivisions in both hemispheres, suggesting similar connectivity-based functions. Bilateral TP subdivisions were thus used in subsequent analyses to investigate their functional preferences and FC-based neonatal and genetic characteristics. This approach aligns with the bilateral, and sometimes redundant, roles of the TP in conceptual knowledge representation[27], although graded hemispheric specializations have also been documented[54] that warrant future investigation. In contrast, whole-brain and ROI-based FC analyses revealed distinct network connections for each TP subdivision: the auditory language network (dorsal TP), the visual paralimbic network (ventromedial TP), and the default semantic network (ventrolateral TP). These results are consistent with the functional preferences of TP subdivisions for auditory/language (dorsal TP), visual/emotional (ventromedial TP) and multimodal (ventrolateral TP) processing. Collectively, these findings highlight the heterogeneous nature of the FC-based TP parcellations in coding information from multiple modalities/sources, facilitating the formation of generalized conceptual representations[9,12,14].

The presence of adult-like TP in the neonatal brain enhances our understanding of the developmental precursors of the TP's role in

https://doi.org/10.1038/s41467-025-58896-y

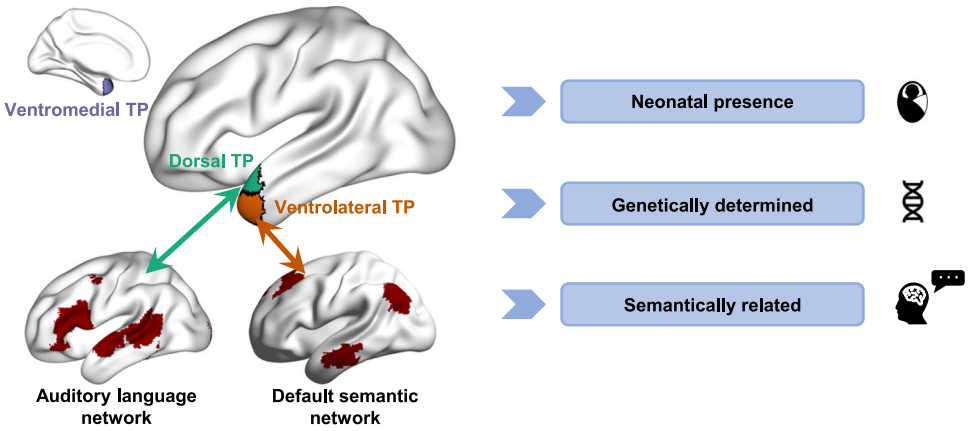

Fig. 6 | Summary of the proposed innate network mechanisms of the temporal pole (TP) in supporting semantic cognition in humans. This figure integrates findings on the neonatally established and genetically influenced functional connectivity characteristics of TP subdivisions and their associations with functional roles in semantic processing, as observed in this study.

semantic neural representation. Utilizing the same data-driven approach applied to adults, we found that functional parcellations in neonates mirror those in adults, providing neurodevelopmental evidence for the functional divisions within the TP[20,21]. Importantly, the adult-like specific FC of the dorsal TP (with the auditory language network) and the ventrolateral TP (with the default semantic network) are evident in neonates, suggesting that neural prewiring supports the contribution of auditory inputs to multimodal conceptual formation from birth. This interpretation aligns the early auditory cortex functioning, starting around the 25th to 29th week of gestation[55], facilitating linguistic exposure in utero. Newborns show selective preferences for human speech over other sounds and can recognize speech patterns (e.g., stress) within the first few days after birth[56–58]. These early speech experiences are linked to early semantic development. Research has shown that pairing the same name with objects (e.g., dinosaurs) varying in color and shape led to the categorization of these objects as the same object, facilitating the formation of generalized concepts, in infants as young as 3-4 months old[59,60]. We propose that the FC characteristics of neonatal TP subdivisions support the early onset of the auditory linguistic role in object knowledge acquisition. This hypothesis is consistent with findings showing the involvement of the dorsal TP in processing speech-derived concrete concepts that are perceptually imperceptible in congenitally blind adults, such as colors and rainbows[61,62]. Additionally, a previous study found delayed responses in the bilateral temporal poles of both 3-month-old infants and adults (after initial activations in the auditory processing areas) during sentence listening[63], suggesting that higher-order functions of the TP, such as semantic processing in adult speech processing[64], are already present in preverbal infants. In summary, the neonatal presence of neighboring TP subdivisions connecting with auditory language and default semantic networks may indicate inborn network characteristics that support multimodal conceptual formation with early access to auditory and speech stimulation.

Adult twin analyses have revealed significant heritable patterns in the specific FC of TP subdivisions that are associated with auditory language comprehension, indicating genetic influences on the FC-based semantic functions of the TP. Previous twin-based studies and GWASs have reported notable heritability in the intrinsic FC characteristics of the language[5,65] and default networks[66,67]. Our results extend this knowledge by showing additional genetic effects on the specialized connections of each network with its corresponding TP subdivision, both at rest and during a comprehension task, providing biological evidence for the distinct functional connections of different TP subdivisions. Moreover, we showed that the FC patterns of the dorsal TP with the auditory language network and the ventrolateral TP with the default semantic network can predict the same subdivision's functional activations and participants' behavioral performance on this comprehension task. These associations reaffirm the established relationships between regional connectivity characteristics and functional relevance[50,68–70]. More importantly, they underscore the genetically programmed functional connections of TP subdivisions in supporting their functional roles in conceptual processing.

The neonatal presence and heritable semantic functions of the specific FC of TP subdivisions provide insights into the innate neural mechanisms underlying human semantic acquisition from early developmental stages. We identified neonatal TP parcellations that show specific FC with the auditory language (dorsal TP) and the default semantic (ventrolateral TP) networks. Although assessing the cognitive relevance of this early-emerging FC in neonates is challenging, their functional roles in conceptual processing in adults, based on associations with functional activations and behavioral performance in a semantic-related task, offer clues. Combining neonatal and twin-based imaging results, we further demonstrate greater genetic influence on specific FC between TP subdivisions and the corresponding network (and ROIs) established in neonates compared to those emerging later in life. These associations suggest early-emerging and long-lasting genetic controls on the neonatal FC characteristics of the TP into adulthood. This interpretation aligns with studies showing higher-order functional networks are more similar among siblings than unrelated children[71] and exhibit genetically-determined individual variances in neonates[72]. These converging findings from various approaches underscore the continuous influence of genetic factors on higher-order cognitive development from early on. Along this line, we speculate on the coherent FC-based semantic functions of TP subdivisions that are operational from the initial developmental stages. While longitudinal investigations are needed to directly link neonatal FC of the TP with later semantic functions, our hypothesis is consistent with multiple lines of evidence highlighting the critical role of the TP in speech-based semantic acquisition. For example, whole-brain FC patterns of the TP in 4- to 18-month-old infants are prospectively associated with their vocabulary size estimated five years later[73], supporting its role in lexico-semantic acquisition. Moreover, the TP, especially its dorsal and ventrolateral subdivisions, is implicated in the fast-mapping process of adults, where semantic knowledge associated with verbal labels is efficiently established through very few exposures[74–76]. It is reasonable to contemplate similar roles of these TP subdivisions, possibly supported by their specific FC with the auditory language and default semantic networks, in the infant fast mapping process, a key mechanism underlying speedy conceptual formation in infancy and early childhood[77–79]. Overall, the early emergence and

genetic basis of the specific FC of TP subdivisions, with their indicative functional roles in semantic acquisition, suggest built-in connectivity mechanisms in the TP as a neurodevelopmental scaffold for multimodal semantic knowledge formation from early on.

Our results also reveal the importance of postnatal experiences in shaping the neural semantic system observed in adulthood. We observed stronger connections of the visual paralimbic networks with the ventromedial TP than with the other two subdivisions in adults. This aligns with previous research showing greater responses of the ventromedial TP to visual stimuli[80] and concrete concepts[62,81], compared to the other TP subdivisions. These findings collectively highlight the neural network mechanisms of the ventromedial TP that underlie visual-related semantic representation. Interestingly, while the ventromedial TP subdivision is topologically similar in neonates and adults, its specific FC with the visual paralimbic network is largely absent in neonates. This implies that these network characteristics develop after birth and may be influenced by postnatal experiences, aligning with the constrained visual input in utero[55]. Therefore, these developmental differences may provide a neurodevelopmental explanation for semantic build-up through postnatal visual and emotional experiences, as postulated by embodied accounts[10,11,82]. Our interpretation is further supported by the presence of shared (resting-state FC) or unique (task-specific FC) environmental effects and the absence of significant genetic effects on the specific FC of the ventromedial TP in adult twins. However, caution should be exercised given the use of a lexicosemantic task potentially minimizing visual-related information processing. Finally, we also observed differences in the neural connections for the dorsal and ventrolateral TP subdivisions between neonates and adults, indicating ongoing development. However, maturational changes in TP parcellations are beyond the scope of this study and could not be optimally investigated due to the cross-sectional nature of the current datasets. Future longitudinal studies are necessary to clarify the developmental trajectory and environmental influences on the neural mechanisms of semantic representation.

Our analyses provide empirical evidence for the early emergence and genetic bases of the functional parcellations within the TP area, yet, several important limitations must be acknowledged. First, although we observed topologically similar TP parcellations based on the same cluster number in both adults and neonates, different optimal cluster numbers were identified for each age group. This discrepancy warrants further investigation. Second, while we demonstrated that the current findings were robust when controlling for tSNR, it remains challenging to recover signal loss during image acquisition through post-imaging processing techniques[83]. Future studies employing multiple-echo acquisitions to mitigate signal dropout, particularly in the inferior temporal regions, are desired[25,84–86]. Third, the functional specificity of the different TP subdivisions in this study was inferred indirectly through Neurosynth-based meta-analytic and FC analyses. Future research should employ experimental tasks specifically targeting semantic processing on information from various modalities and sources, to elucidate the functional significance of the divisional structure of the TP area in the human brain. Forth, the current study only considered the TP area. Given the critical role of the broader ATL area in multimodal semantic processing, this region should be investigated in future research on the development of semantic knowledge.

In conclusion, our analyses of functional imaging data from neonatal and adult twin participants reveal the presence of connectivity-derived functional parcellations of the temporal pole in neonates and associated these inborn connection characteristics with genetic effects on FC-based TP functions in adult semantic processing. The early emergence and genetically guided semantic functions of the specific FC of TP subdivisions indicate inherent network mechanisms underlying its putative hub role in neural semantic representation in the human brain, shedding light on the developmental origins and theoretical modeling of the human semantic system. Broadly speaking, our findings contribute to the growing body of work emphasizing the innate neural roots of central cognitive capacities in humans with protracted developmental trajectories and motivate longitudinal investigations that enable the elucidation of the interplay between nature and nurture through the unfolding of cognitive ability.

Methods

Participants (Table 1)

Adults. Adult images were selected from the HCP 1200 Subjects release (S1200 Release). For the functional parcellations and ROI analyses of the adult TP (Study 1), 100 unrelated adult participants (i.e., from different families) were randomly selected based on the following criteria: 1) completion of four runs of resting-state fMRI images; and 2) less than 10% of volumes with excessive head motion, defined as framewise displacement (FD) ≥ 0.3[87] (mean % of outlier images = 2.74% ± 0.03). Moreover, signal coverage for each ROI was computed for each participant by calculating the percentage of voxels from the ROI that overlapped with the subject-specific brain mask, generated using the 'automask' function from the DPABI toolbox (https://rfmri.org/DPABI). All adult participants in Study 1 demonstrated signal coverage in all relevant ROIs (ROI-specific signal coverage > 0, see the same inclusion criterion in Greene et al.[88]), including the 74 AAL-defined cortical regions, six TP parcellations and 23 neural network ROIs (see Supplementary Table S4 for a summary of ROI-specific signal coverage across all four participant groups). The sample size for the current clustering analyses aligns with previous studies that reported high reliability of parcellation results in the TP[21] and the ATL[89]. For the twin-based analyses of the specific FC of TP subdivisions (Study 3), 190 pairs of twins (123 MZ and 67 DZ) who had four runs of resting-state fMRI images were selected from the HCP twin cohort. Moreover, to assess the functional relevance of the semantic connection patterns of TP subdivisions in conceptual processing and replicate the significant genetic findings (Study 4), 200 pairs of twins (129 MZ and 71 DZ) with available fMRI data for the auditory story comprehension task were further selected. While all twin participants exhibited > 0 ROI-specific signal coverage for all relevant ROIs, head motion was not used as an inclusion criterion to maximize the sample sizes crucial for correlational analyses in twin-based studies (see similar approaches in refs. 90–92). Nonetheless, additional analyses for both Study 3 and 4 confirmed that head motion, including the proportion of outlier images and the mean FD of the remaining volumes after outlier removal, did not significantly differ between MZ and DZ participants (all $p > 0.8$, Supplementary Table S5), and the significant genetic effects on the specific FC of the dorsal and ventrolateral TP subdivisions were obtained independently of head motion influences (Supplementary Table S6). The HCP project was approved by the Institutional Ethics Committee of Washington University in St. Louis, Missouri. All participants signed written informed consent before imaging.

Neonates. A total of 332 neonates were selected from the dHCP dataset (third release) to characterize the functional parcellations and connectivity patterns of the TP in the neonatal brain (Study 2). Imaging data of all included participants were collected within the first month (i.e., ≤ 4 weeks) after birth, and no clinical concerns were observed in the structural images, as evaluated by a perinatal neuroradiologist (radiology score ≤ 3). We applied the same head motion inclusion criteria that were used for the unrelated adult participants in the clustering analyses (Study 1), ensuring that all selected neonates had less than 10% of outlier volumes defined as FD ≥ 0.3 (mean % of outlier images = 4.38% ± 0.03). ROI-specific signal coverage for each neonate was calculated, which were > 0 for all relevant ROIs for all participants. We noted that several ROIs showed suboptimal overlap with the brain masks of some neonates, indicated by minimal ROI-specific signal

coverage <0.1 (Supplementary Table S4). Consequently, we excluded 14 neonates who had at least one ROI with <10% signal coverage, resulting in a revised subset of 318 participants. The neonate-related results were replicated using this revised sample, confirming the reliability of our findings (Supplementary Fig. S7). The dHCP project was approved by the London−Riverside Research Ethics Committee of the Health Research Agency (REC: 14/Lo/1169). Informed parental consent was obtained for imaging acquisition and data release.

Data acquisition

Adults. All adult images were collected at Washington University in St. Louis using a 3 T Connectome Skyra magnetic resonance scanner with a standard 32-channel head coil designed by Siemens. Resting-state and task-based fMRI data were acquired using the same gradient-echo EPI sequence: TR = 720 ms, TE = 33.1 ms, FA = 52°, FOV = 280 × 180 mm^2, voxel size = 2.0 mm isotropic, 72 slices. Four resting-state images were collected over 2 consecutive days (2 runs/day) with opposite phase-encoding directions (right-to-left and left-to-right) for data acquisition on different days. Each run lasted approximately 15 minutes (1200 volumes), during which participants were required to keep their eyes open and fixed on a crosshair projected on a dark background. The story comprehension experiment contained two runs, each with 316 volumes, which were acquired using different phase-encoding directions. High-resolution T1-weighted images were also obtained for every participant using a magnetized rapid gradient-echo (MPRAGE) imaging sequence with TR = 2400 ms, TE = 2.14 ms, reversal time (TI) = 1000 ms, FA = 8°, FOV = 224 × 224 mm^2, voxel size = 0.7 mm isotropic, and total scan time = 7 min and 40 s.

Neonates. Neonatal images were collected at the Evelina Newborn Imaging Centre, St. Thomas' Hospital, London, UK, using a 3 T Philips Achieva (running modified R3.2.2 software) with a neonatal 32-channel phased array head coil[93]. All neonates were scanned during natural sleep. A multiband (MB) 9× accelerated echo-planar imaging sequence lasting 15 minutes was used to obtain the high temporal resolution functional data of neonates (TR = 392 ms, TE = 38 ms, voxel size = 2.15 mm isotropic, 2300 volumes). T2-weighted (TR = 12 s; TE = 156 ms; SENSE factor: axial = 2.11, sagittal = 2.58) and inversion recovery T1-weighted (TR = 4795 ms; TI = 1740 ms; TE = 8.7 ms; SENSE factor: axial = 2.26, sagittal = 2.66) multislice fast spin–echo images were also collected (in-plane resolution = 0.8 × 0.8 mm^2, 1.6 mm slices overlapped by 0.8 mm; see details in ref. 94).

Resting-state image preprocessing

Adults. We used HCP minimally preprocessed fMRI data that were distortion- and motion-corrected and normalized to MNI templates via T1 images[95]. These images were further preprocessed locally using the DPABI toolbox[96], which included 1) linear detrending to minimize low-frequency effects; 2) regression of mean white matter (WM) and cerebrospinal fluid (CSF) signals, continuous head movement[97] (Friston-24 parameters), and outlier scans; 3) temporal bandpass filtering to remove frequencies below 0.01 Hz and above 0.1 Hz; and 4) spatial smoothing with a 6 mm full-width at half-maximum (FWHM) Gaussian filter.

Neonates. The resting-state images of neonates were first minimally preprocessed by dHCP, which included distortion and motion corrections, registration with the corresponding T2w structural image, and ICA denoising using FSL FIX[94]. These images were then normalized to the 40-week T2w templates using the deformational matrices available from the dHCP website. The normalized images of neonates were further preprocessed using the DPABI toolbox, employing the same pipeline as for the adult images, including linear detrending, nuisance regression (WM and CSF signals, continuous head movement, and outlier volumes), temporal bandpass filtering (0.01-0.1 Hz), as well as spatial smoothing (6 mm FWHM).

It is noteworthy that although the unpreprocessed fMRI images of neonates (Study 2, 0.153 ± 0.058 mm) exhibited greater head motion compared to those of adults included in the clustering analyses (Study 1, 0.133 ± 0.023 mm, $t_{430} = 3.34$, $p < 0.001$), a larger proportion of outlier volumes were removed from the neonatal data (4.38% ± 0.03) than from the adult data (2.74% ± 0.03, $t_{430} = 5.26$, $p < 0.001$). As a result, the mean FD of the remaining volumes after outlier removal was smaller in neonates (Study 1, 0.10 ± 0.02 mm) than in adults (Study 2, 0.13 ± 0.02 mm, $t_{430} = 12.83$, $p < 0.001$, Table 1), suggesting effective mitigation of motion effects in the neonatal data.

Functional parcellations in the TP of adult and neonatal brains

A two-level clustering approach (Fig. 1A) was employed to parcellate the TP areas based on the FC patterns of TP voxels with the whole-brain cortical regions defined by the AAL atlas[98]. Subject-specific parcellation maps were first generated using standard K-means clustering techniques. These maps were then subjected to consensus clustering analyses to derive a group-level representative clustering solution[99,100] (MATLAB's Statistics and Machine Learning Toolbox). Specifically, subject-specific FC matrices were generated by performing partial correlations between the time course of each TP voxel and the mean time course of each of the 74 AAL cortical regions. These correlations were transformed to Z scores using Fisher's *r*-to-*z* transformation. A standard K-means clustering algorithm was applied, which treated each observation (i.e., the FC pattern of one TP voxel) as a point in a multidimensional space and iterated cluster assignments of all points 100 times for a given cluster number. The best solution (i.e., optimal clustering results) was determined by minimizing the sum of squared Euclidean distances between each point and the center of its cluster. Individual clustering maps were then processed using a consensus clustering approach to obtain a representative solution at the group level[99–101]. Specifically, a coassignment matrix Q was generated for each participant, where $q_{ij} = 1$ if voxel i and voxel j were assigned to the same cluster, and $q_{ij} = 0$ otherwise. A mean matrix averaged across all participants was generated to reflect the probability of voxel co-assignment. The K-means clustering procedure was then applied to this mean co-assignment matrix to produce the final representative clustering results. The silhouette value was calculated as $(b - a)/\max(a, b)$, where "a" is the average distance between a voxel and other voxels in the same cluster, and "b" is the minimum value of the average distances between a voxel and all voxels from another cluster. Therefore, higher silhouette values indicated greater between-cluster distances than within-cluster distances, suggesting better clustering solutions. To avoid arbitrary decisions on the number of TP subdivisions, the two-level clustering approach was performed for a variety of cluster numbers ranging from $k = 2$ to $k = 8$, with the optimal cluster number determined by the highest silhouette value.

The neonatal TP areas were parcellated using the same two-level clustering approach described above. For each participant, neonatal FC matrices of the TP were similarly computed between each TP voxel and every cerebral cortex defined by the neonatal AAL atlas[102] (also registered to the dHCP templates using ANTs). A cluster number of $k = 3$ was chosen to identify adult-like TP parcellations in the neonatal brain. To assess the topological similarities between TP parcellations in neonates and adults, the TP subdivisions in the adult brain were registered into the neonatal space using ANTs, and the degree of overlapping for overall parcellations and each TP subdivision was evaluated using the Dice coefficient, which measures the ratio of overlapping voxels to the mean voxel number of the compared clusters.

Meta-analyses on the functional preferences of TP subdivisions

The cognitive relevance of the three TP subdivisions was quantitatively surveyed based on the Neurosynth database, which contains 8000

term-based features extracted from the abstracts or text of all included studies[41]. To reduce redundancy among features related to similar topics (e.g., perceptual and perception), latent Dirichlet allocation topic modeling was applied in the Neurosynth database to generate a reduced set of 200 research topics that covered the latent conceptual structure underlying the included literature[103]. A name was determined for each research topic by considering the included terms and their loadings (weights) on this topic. For example, the topic name language comprehension was chosen based on its highest loading terms: language, sentences, and comprehension. Given the current focus on the roles of the TP in cognitive processes, 67 topics pertaining to various mental processes were selected (Supplementary Table S2) after excluding topics related to anatomical landmarks (e.g., inferior parietal lobule, N = 19), methodological terms (e.g., response time, N = 40), atypical populations (e.g., ADHD, N = 13) and unrelated areas (e.g., training, N = 61). Gaussian naïve Bayes classification analyses were used to compute the log odds ratio (LOR), which indexes the log of the ratio between the probability of a given topic in active studies for one TP subdivision (defined as ≥ 5% activated voxels) and that in inactive studies for the same area[41,104]. Thus, the LOR indicates the likelihood that a topic of interest is associated with activation in one TP subdivision. The significance of the association between a specific topic and activation in one TP subdivision (LOR > 0) was derived from permutation tests where a null distribution was generated by permuting the class labels and extracting the LOR for each topic 10000 times.

Network ROI selection

ROIs constituting the neural networks for processing information of different types/modalities were generated based on activation-based meta-analysis results and anatomically defined regions. Specifically, ROIs of the auditory language network were attempted using the terms "language network" and "auditory" in the Neurosynth database. Brain regions generated using the term "auditory" included primary auditory cortices and other temporal regions largely overlapped with those generated using "language network", consistent with the close links between auditory modality and language processing. Therefore, only ROIs identified from the "language network" were considered. The default threshold of FDR corrected $p < 0.01$ with a minimal cluster size of 50 voxels was applied. Seven cerebral regions were identified based on 83 studies (excluding voxels in the cerebellum and TP regions), including the left anterior and posterior middle temporal gyri (LMTGant and LMTGpos), left inferior frontal gyrus (LIFG), left occipital gyrus (LOG), left precentral gyrus (LPreG), and right middle temporal (RMTG) and right occipital gyri (ROG, Fig. 3A).

ROIs forming the default semantic network were similarly generated using the term "default network" (96 studies). A higher cluster size threshold of 100 voxels (FDR corrected $p < 0.01$) was applied to capture the extensive default network typically reported in previous literature[105]. This procedure identified 10 ROIs (excluding the cerebellum and TP voxels), including the bilateral middle temporal gyri (LMTG and RMTG), parahippocampal gyri (LPHG and RPHG), and angular gyri (LAG and RAG); left middle frontal gyrus (LMFG); right superior frontal gyrus (RSFG); and anterior and posterior cingulate cortices (ACC and PCC). These ROIs already encompassed regions important for multimodal semantic representation, such as the angular and middle temporal gyri, aligning with the results of the whole-brain FC analyses in the current study.

For the visual paralimbic network, terms related to "visual" were initially tested but produced extensive activations in the primary visual cortices. Due to challenges in isolating brain regions associated with higher-order visual cognition, the term "concrete" was used, given the predominant role of visual semantics in determining the concreteness of a concept[106]. However, this term generated mixed activations for both concrete and abstract effects in the Neurosynth database, rendering it unsuitable. Therefore, ROIs for the concreteness effect were created based on peak coordinates reported in the meta-analysis by Wang et al.[107] to preferentially process concrete over abstract concepts (radius: 8 mm, overlapping spheres were merged into one ROI). This included four ROIs in the left precuneus gyrus (LPrecuneus), left posterior cingulate cortex (LPCC), left fusiform gyrus (LFG) and left parahippocampal gyrus (LPHG). Moreover, the bilateral olfactory cortices (LOLF and ROLF) within the paralimbic system, which constantly showed strong FC with the ventromedial TP in both our and previous FC results of the TP[20,21], were created based on the AAL atlas and combined with ROIs for the concreteness effect to form the visual paralimbic network. Acknowledging the limited number of studies in Wang et al.[107] (19 studies), an updated visual paralimbic network was defined using visual ROIs defined based on a recent meta-analysis on concrete concepts (72 studies and 1400 participants, Hoffman & Bair[108]). This updated network yielded results consistent with the original findings (Supplementary Materials), supporting their generalizability. To ensure differentiation among networks, overlapping voxels between ROIs from different networks were excluded from both ROIs.

Finally, the FC strength between each TP subdivision and each neural network was computed in two steps: 1) correlations were first calculated between the time course of each TP subdivision (averaged across all voxels within the subdivision, e.g., dorsal TP) and the time course of each ROI (averaged across all included voxels) within a neural network (e.g., the LIFG ROI in the auditory language network); 2) the FC strength between the TP subdivision and the neural network was then obtained by averaging the FC strength of the TP subdivision (e.g., dorsal TP) with all ROIs within the same network (e.g., the 7 ROIs in the auditory language network).

Task-based fMRI data analyses

Univariate analyses. Motion-corrected and normalized functional images generated from the minimally preprocessed pipeline by HCP were first smoothed with a 6 mm FWHM Gaussian filter and then entered into the general linear model (GLM) in SPM 12 (https://www.fil.ion.ucl.ac.uk/spm/software/spm12/) implemented in MATLAB. The GLM included two regressors representing the experimental conditions (i.e., story and math), along with continuous regressors for the 24 head motion parameters and binary regressors for outlier volumes (FD ≥ 0.3, the same head movement parameters applied in the FC analyses) as nuisance variables. After model estimation, neural activation maps associated with language comprehension and arithmetic processing were generated by contrasting the story and math conditions, respectively, with the fixation condition[47,48]. A one-sample *t*-test was performed on the contrast map to characterize the neural correlates of language comprehension and math operation processing at the group level with a significance threshold of FDR corrected $p < 0.05$ and a cluster size of 50 voxels.

Task-specific FC analyses. Before FC estimation, the functional images were preprocessed using the DPABI toolbox, following the same procedure as applied to the resting-state images, including linear detrending; regression of WM, CSF, and head motion; temporal bandpass filtering; and spatial smoothing. The CONN toolbox was then employed to estimate the FC between each TP subdivision and ROIs from the three networks during the story comprehension condition[109,110]. To this end, task-related activations were first estimated based on the GLM, which were removed from the overall signals to generate a residual time series with minimal condition-induced influences. The time series corresponding to the story comprehension and math operation tasks were derived by weighting the residual time series with the task regressor specific to each condition, respectively. A Hanning window was applied to the beginning and ending scans in each block to further decrease potential influences from neighboring blocks. The FC strength between each TP subdivision and each network ROI

was then computed for each condition using Pearson correlations, which were converted into Fisher's Z scores for subsequent analyses.

Support vector regression (SVR) analyses. SVR analyses were performed to evaluate whether the FC patterns of each TP subdivision were associated with its task-specific functional activations and participant's behavioral performance during the auditory language comprehension task, using the LIBSVM package[52] implemented in MATLAB. Specifically, the FC matrices of each TP subdivision with ROIs from the neural network that code the corresponding type of information (e.g., 7 auditory language network ROIs for dorsal TP) were applied as input features for the SVR models. The outcome measures included condition-specific functional activations of the same TP subdivision and participants' behavioral performance. A leave-one-subject-out cross-validation method was used to estimate SVR performance, in which the data of one participant were held out (testing dataset), while the remaining data were used to train the SVR model. The trained model was then applied to the FC matrix of the same TP subdivision in the testing dataset to produce the predicted activation degree in the TP subdivision of this participant. Once the data from every participant were used as the testing dataset to generate the predicted activation degrees of this TP subdivision, Pearson's correlation was calculated between the predicted and true activation degrees across all participants to determine the SVR prediction performance. The significance of the prediction performance was determined by permutation tests with randomized connectivity-activation/behavioral performance associations (N = 10000).

Twin-based analyses

To estimate the heritability of a phenotype, we utilized twin-based analyses that leverage the genetic and environmental similarities between twins. MZ twins share 100% of their genetic makeup, while DZ twins share 50%. Both types of twins typically share 100% of their environment when living in the same household[111]. By examining the differences in interclass correlations between MZ and DZ twins, we can decompose phenotypic variances into A, C, and E factors. We conducted SEM analyses to statistically estimate the genetic and environmental contributions to individual differences in the specific FC of each TP subdivision using the umx package[112] implemented in R. Both the full ACE model and the submodels (AE, CE and E models) were examined with age and sex as covariates. Parameters in each model were estimated using maximum likelihood, and the Akaike information criterion (AIC) was calculated to assess model fit, balancing model parsimony and goodness of fit. The model with the lowest AIC value was considered the optimal fit. If an AE or CE model was selected, it was further compared to the E model using χ^2 tests to determine the significance of the additive genetic (a^2) or common environmental (c^2) effects in the corresponding model (see the similar approach in refs. 32,113,114).

Permutation tests using the full ACE model were conducted to estimate the significance of the additive genetic (a^2) or common environmental (c^2) effect, in order to validate our model choice in the SEM analyses and to compare the differences between these two factors for each TP subdivision[91]. During each iteration, the MZ/DZ labels and the composition of twin pairs were shuffled so that each MZ or DZ twin pair contained two randomly selected participants. The sex and age (in years) of these randomly assigned twin pairs were kept constant, maintaining their inclusion as covariates in the model estimation. This procedure was repeated 10,000 times, producing null distributions for a^2, c^2, and a^2-c^2 (or c^2-a^2), based on which the significance of a^2, c^2 and their differences derived from the true data could be determined.

Reporting summary

Further information on research design is available in the Nature Portfolio Reporting Summary linked to this article.

Data availability

The images of the HCP (adults, including both unrelated and twin participants) and dHCP (neonates) datasets are available at https://www.humanconnectome.org/ and https://www.developingconnectome.org, respectively. In adherence to the privacy policies of both datasets, the preprocessed images of both adult and neonatal participants, including their IDs, could only be shared upon request with qualified investigators who agree to the Restricted Data Use Terms associated with these two projects. The Neurosynth dataset is available at https://github.com/neurosynth/neurosynth-data. The 40-week templates can be downloaded at https://git.fmrib.ox.ac.uk/seanf/dhcp-resources/-/blob/master/docs/dhcp-augmented-volumetric-atlas-extended.md#download-42-gb. The identified functional parcellations in the TP areas and the neural network masks applied in the ROI analyses are available at https://github.com/Ziliang-Zhu/TP_neonatal_twins_code/tree/main. Source data are provided with this paper.

Code availability

Software packages used in this study include DPABI V5.1 (https://rfmri.org/DPABI), SPM12 (https://www.fil.ion.ucl.ac.uk/spm/software/spm12/), CONN v17 (https://web.conn-toolbox.org/), REST V1.8 (https://rfmri.org/REST), BrainNet Viewer v1.7 (http://www.nitrc.org/projects/bnv/), LIBSVM 3.22 (https://www.csie.ntu.edu.tw/~cjlin/libsvm/), neurosynth package (version 0.3.4; https://github.com/neurosynth/neurosynth), nilearn package (version 0.10.2; https://github.com/nilearn/nilearn/), umx package (version 4.15.1; https://cran.r-project.org/web/packages/umx/index.html), ANTs (version 2.3.4.dev203-g952e7; http://stnava.github.io/ANTs/), MATLAB 2018a (https://www.mathworks.com/products/matlab.html), Python 2.7 (https://www.python.org/download/releases/2.7/), Python 3.9 (https://www.python.org), RStudio (version 2022.07.2 + 576; https://posit.co/products/open-source/rstudio/), JASP 0.17.2.1 (https://jasp-stats.org/download/). The codes and ROI files for the analyses in this study[115] are available at https://github.com/Ziliang-Zhu/TP_neonatal_twins_code/tree/main.

References

1. Darwin, C. *The descent of man: and selection in relation to sex*. (John Murray, Albemarle Street., 1888).
2. Heyes, C. New thinking: the evolution of human cognition. *Philos. Trans. R. Soc. B: Biol. Sci.* **367**, 2091–2096 (2012).
3. Spelke, E. S. *What Babies Know: Core Knowledge and Composition Volume 1*. Vol. 1 (Oxford University Press, 2022).
4. King, M. J., Katz, D. P., Thompson, L. A. & Macnamara, B. N. Genetic and environmental influences on spatial reasoning: A meta-analysis of twin studies. *Intelligence* **73**, 65–77 (2019).
5. Mekki, Y. et al. The genetic architecture of language functional connectivity. *NeuroImage*, 118795 (2021).
6. Carrión-Castillo, A., Paz-Alonso, P. M. & Carreiras, M. Brain structure, phenotypic and genetic correlates of reading performance. *Nat. Hum. Behav.* **7**, 1120–1134 (2023).
7. Eising, E. et al. Genome-wide analyses of individual differences in quantitatively assessed reading- and language-related skills in up to 34,000 people. *Proc. Natl Acad. Sci. USA* **119**, e2202764119 (2022).
8. Block, N. A confusion about innateness. *Behav. Brain Sci.* **2**, 27–29 (1979).
9. Bi, Y. Dual coding of knowledge in the human brain. *Trends Cogn. Sci.* **25**, 883–895 (2021).
10. Barsalou, L. W. On staying grounded and avoiding quixotic dead ends. *Psychonomic Bull. Rev.* **23**, 1122–1142 (2016).
11. Martin, A. GRAPES—Grounding representations in action, perception, and emotion systems: How object properties and categories are represented in the human brain. *Psychonomic Bull. Rev.* **23**, 979–990 (2016).

12. Lambon Ralph, M. A., Jefferies, E., Patterson, K. & Rogers, T. T. The neural and computational bases of semantic cognition. *Nat. Rev. Neurosci.* **18**, 42–55 (2017).
13. Binder, J. R., Desai, R. H., Graves, W. W. & Conant, L. L. Where is the semantic system? A critical review and meta-analysis of 120 functional neuroimaging studies. *Cereb. Cortex* **19**, 2767–2796 (2009).
14. Patterson, K., Nestor, P. J. & Rogers, T. T. Where do you know what you know? The representation of semantic knowledge in the human brain. *Nat. Rev. Neurosci.* **8**, 976–987 (2007).
15. Davies, R. R., Halliday, G. M., Xuereb, J. H., Kril, J. J. & Hodges, J. R. The neural basis of semantic memory: Evidence from semantic dementia. *Neurobiol. Aging* **30**, 2043–2052 (2009).
16. Herlin, B., Navarro, V. & Dupont, S. The temporal pole: from anatomy to function-A literature appraisal. *Journal of Chemical Neuroanatomy*, 101925 (2021).
17. Lambon Ralph, M. A., Pobric, G. & Jefferies, E. Conceptual knowledge is underpinned by the temporal pole bilaterally: Convergent evidence from rTMS. *Cereb. Cortex* **19**, 832–838 (2008).
18. Pobric, G., Jefferies, E. & Ralph, M. A. L. Anterior temporal lobes mediate semantic representation: Mimicking semantic dementia by using rTMS in normal participants. *Proc. Natl Acad. Sci. USA* **104**, 20137–20141 (2007).
19. Pobric, G., Jefferies, E. & Lambon Ralph, M. A. Amodal semantic representations depend on both anterior temporal lobes: Evidence from repetitive transcranial magnetic stimulation. *Neuropsychologia* **48**, 1336–1342 (2010).
20. Fan, L. et al. Connectivity-based parcellation of the human temporal pole using diffusion tensor imaging. *Cereb. Cortex* **24**, 3365–3378 (2014).
21. Pascual, B. et al. Large-scale brain networks of the human left temporal pole: A functional connectivity MRI Study. *Cereb. Cortex* **25**, 680–702 (2015).
22. Binney, R. J., Parker, G. J. M. & Lambon Ralph, M. A. Convergent connectivity and graded specialization in the rostral human temporal lobe as revealed by diffusion-weighted imaging probabilistic tractography. *J. Cogn. Neurosci.* **24**, 1998–2014 (2012).
23. Hung, J., Wang, X., Wang, X. & Bi, Y. Functional subdivisions in the anterior temporal lobes: a large scale meta-analytic investigation. *Neurosci. Biobehav. Rev.* **115**, 134–145 (2020).
24. Jackson, R. L., Bajada, C. J., Rice, G. E., Cloutman, L. L. & Lambon Ralph, M. A. An emergent functional parcellation of the temporal cortex. *NeuroImage* **170**, 385–399 (2018).
25. Jackson, R. L., Hoffman, P., Pobric, G. & Lambon Ralph, M. A. The semantic network at work and rest: Differential connectivity of anterior temporal lobe subregions. *J. Neurosci.* **36**, 1490–1501 (2016).
26. Plaut, D. C. Graded modality-specific specialisation in semantics: A computational account of optic aphasia. *Cogn. Neuropsychol.* **19**, 603–639 (2002).
27. Rice, G. E., Lambon Ralph, M. A. & Hoffman, P. The roles of left versus right anterior temporal lobes in conceptual knowledge: An ALE meta-analysis of 97 functional neuroimaging studies. *Cereb. Cortex* **25**, 4374–4391 (2015).
28. Huth, A. G., De Heer, W. A., Griffiths, T. L., Theunissen, F. E. & Gallant, J. L. Natural speech reveals the semantic maps that tile human cerebral cortex. *Nature* **532**, 453–458 (2016).
29. Mahon, B. Z. & Caramazza, A. Concepts and categories: A cognitive neuropsychological perspective. *Annu. Rev. Psychol.* **60**, 27–51 (2009).
30. Kosakowski, H. L. et al. Selective responses to faces, scenes, and bodies in the ventral visual pathway of infants. *Curr. Biol.* **32**, 265–274.e265 (2022).
31. Deen, B. et al. Organization of high-level visual cortex in human infants. *Nat. Commun.* **8**, 13995 (2017).
32. Abbasi, N., Duncan, J. & Rajimehr, R. Genetic influence is linked to cortical morphology in category-selective areas of visual cortex. *Nature Communications* **11** (2020).
33. Van Essen, D. C. et al. The WU-minn human connectome project: An overview. *NeuroImage* **80**, 62–79 (2013).
34. Makropoulos, A. et al. The developing human connectome project: A minimal processing pipeline for neonatal cortical surface reconstruction. *NeuroImage* **173**, 88–112 (2018).
35. Desikan, R. S. et al. An automated labeling system for subdividing the human cerebral cortex on MRI scans into gyral based regions of interest. *NeuroImage* **31**, 968–980 (2006).
36. Ding, S.-L., Van Hoesen, G. W., Cassell, M. D. & Poremba, A. Parcellation of human temporal polar cortex: A combined analysis of multiple cytoarchitectonic, chemoarchitectonic, and pathological markers. *J. Comp. Neurol.* **514**, 595–623 (2009).
37. Buckner, R. L., Andrews-Hanna, J. R. & Schacter, D. L. in *The year in cognitive neuroscience 2008*. *Annals of the New York Academy of Sciences*. 1-38 (Blackwell Publishing, 2008).
38. Raichle, M. E. The brain's default mode network. *Annu. Rev. Neurosci.* **38**, 433–447 (2015).
39. Yeo, B. T. et al. The organization of the human cerebral cortex estimated by intrinsic functional connectivity. *J. Neurophysiol.* **106**, 1125–1165 (2011).
40. Jackson, R. L. The neural correlates of semantic control revisited. *NeuroImage* **224**, 117444 (2021).
41. Yarkoni, T., Poldrack, R. A., Nichols, T. E., Van Essen, D. C. & Wager, T. D. Large-scale automated synthesis of human functional neuroimaging data. *Nat. Methods* **8**, 665–670 (2011).
42. Gazzaniga M. S., George R. B. I. Mangun R. *Cognitive neuroscience: The biology of the mind*. (The MIT Press, 2014).
43. Mesulam, M.-M. *Principles of behavioral and cognitive neurology*. (Oxford University Press, 2000).
44. Blond, B. N., Fredericks, C. A. & Blumberg, H. P. Functional neuroanatomy of bipolar disorder: structure, function, and connectivity in an amygdala–anterior paralimbic neural system. *Bipolar Disord.* **14**, 340–355 (2012).
45. Avants, B. B., Tustison, N. & Song, G. Advanced normalization tools (ANTS). *Insight j.* **2**, 1–35 (2009).
46. Binder, J. R. et al. Mapping anterior temporal lobe language areas with fMRI: A multicenter normative study. *NeuroImage* **54**, 1465–1475 (2011).
47. Glasser, M. F. et al. A multi-modal parcellation of human cerebral cortex. *Nature* **536**, 171–178 (2016).
48. Rajimehr, R., Firoozi, A., Rafipoor, H., Abbasi, N. & Duncan, J. Complementary hemispheric lateralization of language and social processing in the human brain. *Cell Rep.* **41** (2022).
49. Norman, K. A., Polyn, S. M., Detre, G. J. & Haxby, J. V. Beyond mind-reading: multi-voxel pattern analysis of fMRI data. *Trends Cogn. Sci.* **10**, 424–430 (2006).
50. Saygin, Z. M. et al. Connectivity precedes function in the development of the visual word form area. *Nat. Neurosci.* **19**, 1250–1255 (2016).
51. Saygin, Z. M. et al. Anatomical connectivity patterns predict face selectivity in the fusiform gyrus. *Nat. Neurosci.* **15**, 321–327 (2012).
52. Chang, C.-C. & Lin, C.-J. LIBSVM: a library for support vector machines. *ACM Trans. Intell. Syst. Technol. (TIST)* **2**, 1–27 (2011).
53. Wang, X. et al. Physical distance to sensory-motor landmarks predicts language function. *Cerebral Cortex* **33**, 10.1093/cercor/bhac344 (2023).
54. Gainotti, G. Is the difference between right and left ATLs due to the distinction between general and social cognition or between verbal and non-verbal representations? *Neurosci. Biobehav. Rev.* **51**, 296–312 (2015).

55. Meredith Weiss, S., Aydin, E., Lloyd-Fox, S. & Johnson, M. H. Trajectories of brain and behaviour development in the womb, at birth and through infancy. *Nat. Hum. Behav.* **8**, 1251–1262 (2024).
56. Kuhl, P. K. Early language acquisition: cracking the speech code. *Nat. Rev. Neurosci.* **5**, 831–843 (2004).
57. Sansavini, A., Bertoncini, J. & Giovanelli, G. Newborns discriminate the rhythm of multisyllabic stressed words. *Developmental Psychol.* **33**, 3 (1997).
58. Vouloumanos, A. & Werker, J. F. Listening to language at birth: evidence for a bias for speech in neonates. *Developmental Sci.* **10**, 159–164 (2007).
59. Ferry, A. L., Hespos, S. J. & Waxman, S. R. Categorization in 3-and 4-month-old infants: an advantage of words over tones. *Child Dev.* **81**, 472–479 (2010).
60. Ferguson, B. & Waxman, S. Linking language and categorization in infancy. *J. Child Lang.* **44**, 527–552 (2017).
61. Wang, X., Men, W., Gao, J., Caramazza, A. & Bi, Y. Two forms of knowledge representations in the human brain. *Neuron* **107**, 383–393.e385 (2020).
62. Striem-Amit, E., Wang, X., Bi, Y. & Caramazza, A. Neural representation of visual concepts in people born blind. *Nature Communications* **9** (2018).
63. Dehaene-Lambertz, G. et al. Functional organization of perisylvian activation during presentation of sentences in preverbal infants. *Proc. Natl Acad. Sci. USA* **103**, 14240–14245 (2006).
64. Fedorenko, E., Blank, I. A., Siegelman, M. & Mineroff, Z. Lack of selectivity for syntax relative to word meanings throughout the language network. *Cognition* **203**, 104348 (2020).
65. Wen, H., Wang, D., & Bi, Y. Processing language partly shares neural genetic basis with processing tools and body parts. *eNeuro* **11**, 10.1523/ENEURO.0138-24.2024 (2024).
66. Ge, T., Holmes, A. J., Buckner, R. L., Smoller, J. W. & Sabuncu, M. R. Heritability analysis with repeat measurements and its application to resting-state functional connectivity. *Proc. Natl Acad. Sci. USA* **114**, 5521–5526 (2017).
67. Glahn, D. C. et al. Genetic control over the resting brain. *Proc. Natl Acad. Sci. USA* **107**, 1223–1228 (2010).
68. Cohen, A. L. et al. Defining functional areas in individual human brains using resting functional connectivity MRI. *Neuroimage* **41**, 45–57 (2008).
69. Gordon, E. M. et al. Generation and evaluation of a cortical area parcellation from resting-state correlations. *Cereb. cortex* **26**, 288–303 (2016).
70. Mars, R. B., Passingham, R. E. & Jbabdi, S. Connectivity Fingerprints: From Areal Descriptions to Abstract Spaces. *Trends Cogn. Sci.* **22**, 1026–1037 (2018).
71. Miranda-Dominguez, O. et al. Heritability of the human connectome: A connectotyping study. *Netw. Neurosci.* **2**, 175–199 (2018).
72. Molloy, M. F. & Saygin, Z. M. Individual variability in functional organization of the neonatal brain. *NeuroImage* **253**, 119101 (2022).
73. Yu, X. et al. Functional Connectivity in Infancy and Toddlerhood Predicts Long-Term Language and Preliteracy Outcomes. *Cerebral Cortex*, 10.1093/cercor/bhab230 (2021).
74. Atir-Sharon, T., Gilboa, A., Hazan, H., Koilis, E. & Manevitz, L. M. Decoding the formation of new semantics: MVPA investigation of rapid neocortical plasticity during associative encoding through fast mapping. *Neural plasticity* **2015**, 804385 (2015).
75. Merhav, M., Karni, A. & Gilboa, A. Not all declarative memories are created equal: fast mapping as a direct route to cortical declarative representations. *Neuroimage* **117**, 80–92 (2015).
76. Vukovic, N., Hansen, B., Lund, T. E., Jespersen, S. & Shtyrov, Y. Rapid microstructural plasticity in the cortical semantic network following a short language learning session. *PLoS Biol.* **19**, e3001290 (2021).
77. Carey, S. & Bartlett, E. Acquiring a single new word. *Pap. Rep. Child Lang. Dev.* **15**, 13 (1978).
78. Houston-Price, C., Plunkett, K. & Harris, P. 'Word-learning wizardry'at 1; 6. *J. Child Lang.* **32**, 175–189 (2005).
79. Torkildsen, J. V. K. et al. Productive vocabulary size predicts event-related potential correlates of fast mapping in 20-month-olds. *J. Cogn. Neurosci.* **20**, 1266–1282 (2008).
80. Visser, M., Jefferies, E., Embleton, K. V. & Lambon Ralph, M. A. Both the middle temporal gyrus and the ventral anterior temporal area are crucial for multimodal semantic processing: Distortion-corrected fMRI Evidence for a double gradient of information convergence in the temporal lobes. *J. Cogn. Neurosci.* **24**, 1766–1778 (2012).
81. Hoffman, P., Binney, R. J. & Lambon Ralph, M. A. Differing contributions of inferior prefrontal and anterior temporal cortex to concrete and abstract conceptual knowledge. *Cortex* **63**, 250–266 (2015).
82. Pulvermüller, F. How neurons make meaning: brain mechanisms for embodied and abstract-symbolic semantics. *Trends Cogn. Sci.* **17**, 458–470 (2013).
83. Manso Jimeno, M., Vaughan, J. T. & Geethanath, S. Superconducting magnet designs and MRI accessibility: A review. *NMR Biomedicine* **36**, e4921 (2023).
84. Poser, B. A. & Norris, D. G. Investigating the benefits of multi-echo EPI for fMRI at 7 T. *Neuroimage* **45**, 1162–1172 (2009).
85. Poser, B. A. & Norris, D. G. Fast spin echo sequences for BOLD functional MRI. *Magn. Reson. Mater. Phys., Biol. Med.* **20**, 11–17 (2007).
86. Halai, A. D., Welbourne, S. R., Embleton, K. & Parkes, L. M. A comparison of dual gradient-echo and spin-echo fMRI of the inferior temporal lobe. *Hum. Brain Mapp.* **35**, 4118–4128 (2014).
87. Power, J. D., Barnes, K. A., Snyder, A. Z., Schlaggar, B. L. & Petersen, S. E. Spurious but systematic correlations in functional connectivity MRI networks arise from subject motion. *NeuroImage* **59**, 2142–2154 (2012).
88. Greene, A. S. et al. Brain–phenotype models fail for individuals who defy sample stereotypes. *Nature* **609**, 109–118 (2022).
89. Persichetti, A. S., Denning, J. M., Gotts, S. J. & Martin, A. A data-driven functional mapping of the anterior temporal lobes. *J. Neurosci.* (2021).
90. Anderson, K. M. et al. Heritability of individualized cortical network topography. *Proc. Natl Acad. Sci. USA* **118**, 10.1073/pnas.2016271118 (2021).
91. Colclough, G. L. et al. The heritability of multi-modal connectivity in human brain activity. *eLife* **6**, 10.7554/eLife.20178 (2017).
92. Ribeiro, F. L., Dos Santos, F. R. C., Sato, J. R., Pinaya, W. H. L. & Biazoli, C. E. Inferring the heritability of large-scale functional networks with a multivariate ACE modeling approach. *Netw. Neurosci.* **5**, 527–548 (2021).
93. Hughes, E. J. et al. A dedicated neonatal brain imaging system. *Magn. Reson. Med.* **78**, 794–804 (2017).
94. Fitzgibbon, S. P. et al. The developing human connectome project (dHCP) automated resting-state functional processing framework for newborn infants. *NeuroImage* **223**, 117303 (2020).
95. Glasser, M. F. et al. The minimal preprocessing pipelines for the human connectome project. *NeuroImage* **80**, 105–124 (2013).
96. Yan, C.-G., Wang, X.-D., Zuo, X.-N. & Zang, Y.-F. DPABI: Data processing & analysis for (resting-state) brain imaging. *Neuroinformatics* **14**, 339–351 (2016).
97. Friston, K. J., Williams, S., Howard, R., Frackowiak, R. S. J. & Turner, R. Movement-related effects in fMRI time-series. *Magn. Reson. Med.* **35**, 346–355 (1996).
98. Tzourio-Mazoyer, N. et al. Automated anatomical labeling of activations in SPM using a macroscopic anatomical parcellation of the MNI MRI single-subject brain. *Neuroimage* **15**, 273–289 (2002).

99. Guedj, C. & Vuilleumier, P. Functional connectivity fingerprints of the human pulvinar: Decoding its role in cognition. *NeuroImage* **221**, 117162 (2020).
100. Monti, S., Tamayo, P., Mesirov, J. & Golub, T. Consensus clustering: a resampling-based method for class discovery and visualization of gene expression microarray data. *Mach. Learn.* **52**, 91–118 (2003).
101. Janssen, R. J., Jylänki, P., Kessels, R. P. C. & van Gerven, M. A. J. Probabilistic model-based functional parcellation reveals a robust, fine-grained subdivision of the striatum. *NeuroImage* **119**, 398–405 (2015).
102. Shi, F. et al. Infant Brain Atlases from Neonates to 1- and 2-Year-Olds. *PLoS ONE* **6**, e18746 (2011).
103. Blei, D. M., Ng, A. Y. & Jordan, M. I. Latent dirichlet allocation. *J. Mach. Learn. Res.* **3**, 993–1022 (2003).
104. de la Vega, A., Chang, L. J., Banich, M. T., Wager, T. D. & Yarkoni, T. Large-scale meta-analysis of human medial frontal cortex reveals tripartite functional organization. *J. Neurosci.* **36**, 6553–6562 (2016).
105. Smallwood, J. et al. The default mode network in cognition: a topographical perspective. *Nat. Rev. Neurosci.* **22**, 503–513 (2021).
106. Connell, L. & Lynott, D. Strength of perceptual experience predicts word processing performance better than concreteness or imageability. *Cognition* **125**, 452–465 (2012).
107. Wang, J., Conder, J. A., Blitzer, D. N. & Shinkareva, S. V. Neural representation of abstract and concrete concepts: A meta-analysis of neuroimaging studies. *Hum. Brain Mapp.* **31**, 1459–1468 (2010).
108. Hoffman, P. & Bair, M. Neural specialisation for concrete and abstract concepts revealed through meta-analysis. Preprint at *bioRxiv* https://doi.org/10.1101/2024.07.11.603079 (2024).
109. Chai, X. J., Castañón, A. N., Öngür, D. & Whitfield-Gabrieli, S. Anticorrelations in resting state networks without global signal regression. *Neuroimage* **59**, 1420–1428 (2012).
110. Whitfield-Gabrieli, S. & Nieto-Castanon, A. Conn: a functional connectivity toolbox for correlated and anticorrelated brain networks. *Brain connectivity* **2**, 125–141 (2012).
111. Rijsdijk, F. V. Analytic approaches to twin data using structural equation models. *Brief. Bioinforma.* **3**, 119–133 (2002).
112. Bates, T. C., Maes, H. & Neale, M. C. umx: twin and path-based structural equation modeling in R. *Twin Res. Hum. Genet.* **22**, 27–41 (2019).
113. Jiang, N. et al. Negative parenting affects adolescent internalizing symptoms through alterations in amygdala-prefrontal circuitry: a longitudinal twin study. *Biol. Psychiatry* **89**, 560–569 (2021).
114. Sanchez, J. F. Q., Liu, X., Zhou, C. & Hildebrandt, A. Nature and nurture shape structural connectivity in the face processing brain network. *NeuroImage* **229**, 117736 (2021).
115. Zhu, Z. et al. Innate network mechanisms of temporal pole for semantic cognition in neonatal and adult twin studies. *Zenodo*, https://doi.org/10.5281/zenodo.15074861 (2025)

Acknowledgements

This work was supported by the STI2030-Major Project (#2021ZD0200500 to X.Y., #2021ZD0204100 to Y.B.), the National Natural Science Foundation of China (#32100867 awarded to X.Y., #31925020 awarded to Y.B., #32100837 awarded to H.Y., #32171089 awarded to Y.H.), the Fundamental Research Funds for the Central Universities #2233300005 (awarded to Y.B.), and the China Postdoctoral Science Foundation #2024M760231 (awarded to H.W.). Human adult data was provided by the Human Connectome Project, WU-Minn Consortium (Principal Investigators: David Van Essen and Kamil Ugurbil; 1U54MH091657) funded by the 16 NIH Institutes and Centers that support the NIH Blueprint for Neuroscience Research; and by the McDonnell Center for Systems Neuroscience at Washington University. The human neonate data were provided by the developing Human Connectome Project, KCL-Imperial-Oxford Consortium funded by the European Research Council under the European Union Seventh Framework Programme (FP/2007-2013) / ERC Grant Agreement no. [319456]. The Neurosynth dataset was provided by Tal Yarkoni. We thank the investigative teams and researchers providing these publicly available datasets, as well as the funding agencies supporting the availability of these datasets. We would also like to acknowledge the assistance of Xiaosha Wang, Nan Lin, Xiuyi Wang, Jianlong Zhao, Shuang Tian, Xiaohui You in theoretical development, result visualization and code validation.

Author contributions

Z. Z., H. Y., Y. B. and X. Y. designed the research. Z. Z. and H. Y. conducted the research. H. W., J. H. and Y. H. provide analytical support. Z. Z. and X. Y. wrote the original draft of the manuscript, and all authors contributed to review and editing. X. Y. and Y. B. supervised the project.

Competing interests

The authors declare no competing interests.

Additional information

Supplementary information The online version contains supplementary material available at https://doi.org/10.1038/s41467-025-58896-y.

Correspondence and requests for materials should be addressed to Yanchao Bi or Xi Yu.

Peer review information *Nature Communications* thanks Rebecca Jackson, Rhodri Cusack, and the other, anonymous, reviewer(s) for their contribution to the peer review of this work. A peer review file is available.